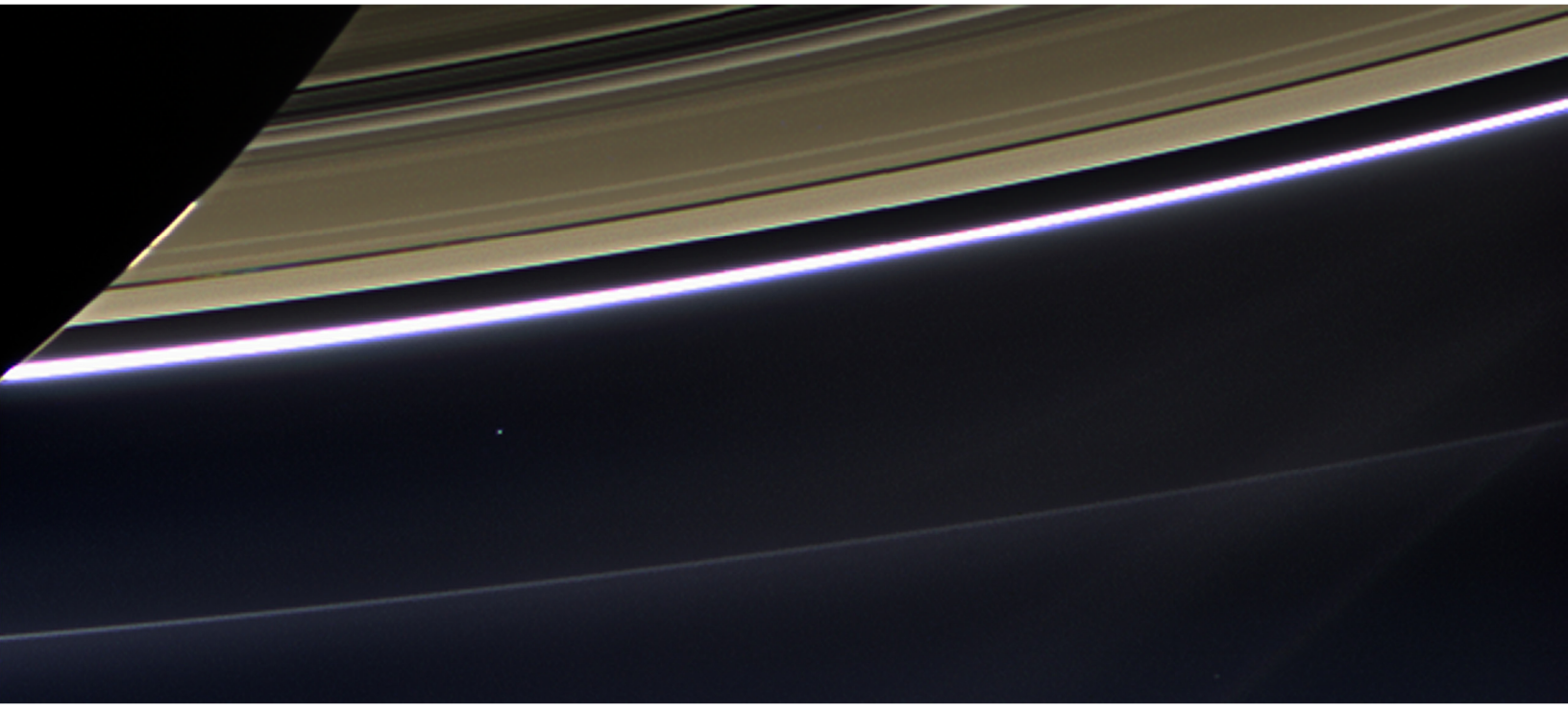

RINGS

Scientists had never before studied the particle size, temperature, composition and dynamics of Saturn's rings from Saturn orbit. Cassini discovered new rings, captured extraordinary ring-moon interactions, observed the lowest ring-temperature ever recorded at Saturn, discovered that the moon Enceladus is the source for Saturn's E-ring, and viewed the rings at equinox when sunlight strikes the rings edge-on, revealing never-before-seen ring features and details. Cassini data have swayed the lively debate over the age of the rings in favor of young rings.

The Ring Working Group (RWG) actively coordinated and enabled Cassini ring observations throughout the mission. Cassini has rewritten the textbooks regarding our understanding of Saturn's Rings, a full generation after Voyager first revealed their complex structure. Not only were all key science objectives successfully accomplished over the course of the Cassini mission, but a number of new science objectives were formulated and addressed along the way, either in response to unexpected results or capitalizing on observational opportunities. The Grand Finale orbits opened up new science opportunities not originally envisioned. There is no question that the science return of Cassini vastly exceeded the expectations as described in the original announcement of opportunity.

CONTENTS

Figures

Tables

EXECUTIVE SUMMARY

… the rings are changing before our eyes dynamically and they are much younger than the solar system compositionally.

Cassini has rewritten the textbooks regarding our understanding of Saturn's Rings, a full generation after Voyager first revealed their complex structure. In fact, Cassini studies of Saturn's rings have already been thoroughly reviewed in two sets of review chapters and articles. In the first major review volume, Saturn after Cassini-Huygens, very thorough reviews are given by Colwell et al. [2009]; Charnoz et al. [2009]; Cuzzi et al. [2009]; Horanyi et al. [2009]; and Schmidt et al. [2009], which remain largely valid as of this writing even if they predate many important results. A short, nonspecialist review is given by Cuzzi et al. [2010]. More recent complete reviews can be found in the Cambridge Planetary Rings book, including Cassini's results prior to the Ring-Grazing and Grand Finale orbits [Charnoz et al. 2018; Cuzzi et al. 2018a; Estrada et al. 2018; Hedman et al. 2018a; Murray and French 2018; Nicholson et al. 2018; Spahn et al. 2018; Spilker et al. 2018]. Finally, Section 3.2 Instrument Science Results updates the story to the very end of the mission, including results from Cassini's last moments and chapters with exhaustive bibliographies. We attempt to cover the highlights of ring science from beginning to end of the mission as organized by our own goals and objectives, and in a readable way we provide a thread of continuity connecting Cassini's vast accomplishments to the big picture of ring origin and evolution. In summary, the rings are changing before our eyes dynamically and they are much younger than the solar system compositionally. Following is a list of our top 20 highlights.

Waves and Collective Dynamics

Spiral density and bending waves were discovered by Voyager. They are driven at orbital resonances with various satellites, blanket the A-ring, and are sprinkled throughout the B-ring and C-ring. Improved analysis tools have allowed even the weakest of these features to be studied in detail, and they provide powerful constraints on the underlying, local surface mass density on several-km spatial scales. About a dozen spiral density and bending waves in the C-ring have been shown to be caused by gravitational and pressure modes inside the planet, and most recently, even constrain the interior structure of Saturn and its rotation rate.

Ring microstructure on sub-km scales is seen everywhere by stellar and radio occultations, and varies on short timescales. Ubiquitous transient gravitational instabilities called self-gravity wakes arise and are torn apart by differential rotation. These wakes vary in configuration across the rings, and their properties imply a ring vertical thickness of tens of meters or less. An unrelated axisymmetric kind of microstructure, due more to viscous forces than self-gravity, can also be seen at various places in the denser parts of the rings. Images taken from close orbits, with sub-km resolution, show that fine-scale structure is widespread in optically thick regions (some of it granular and some axisymmetric or streaky). Dense clumps called straw, each the size of a convoy of aircraft

carriers, are seen in between the dense crests of strong spiral density waves, are probably compacted as particles pass through the crests, and are subsequently broken apart by collisions.

Embedded Moonlets

Analysis of Cassini images have now shown that skirted, embedded 10 km size moonlets are responsible for opening both the Encke and Keeler gaps in the A-ring (see the Icy Satellites chapter). In general, the small ringmoons lying within and near to the rings have very low densities and are likely rubble piles with dense cores. However, moonlets have not been found in similar gaps in the Cassini Division or C-ring with the ~1 km sizes previously thought necessary to clear them.

Flocks of smaller propeller objects of 100–200 m size, detectable only in their disturbance of nearby ring material, occupy three radial bands in the A-ring. A dozen or so of the largest of these objects, 0.1–1 km in size, wander in semi-major axis, perhaps because of gravitational scattering by the clumpy ring material they interact with. Discrete km-size objects have also been inferred from disturbances at the outer edges of the A-ring and B-ring and in the Huygens ringlet of the Cassini Division. One such object has been imaged in the B-ring. Some of these objects seem to disaggregate and perhaps reaggregate in place, on timescales of months or years, suggesting ongoing recycling of material driven by satellite forcing, self-gravity, and collisions.

Rings in 3-D

Cassini discovered dramatic vertical distortions of the rings, in addition to the well-known spiral bending waves, near Equinox when the sun's illumination was at a grazing angle. The edges of the Keeler gap are noticeably warped, consistent with the small inclination of its central ringmoon Daphnis, but those of the Encke gap are not. The outer edge of the B-ring showed alpen-like, spiky peaks and shadows. The outer edge of the A-ring showed a very clumpy structure, lacking distinct peaks, but with shadows suggesting vertical relief.

Ring Particle Properties

Voyager showed that the main ring particle size distributions tend towards powerlaws ranging between cm-m radii. Cassini has shown that the slope and the minimum and maximum sizes of these powerlaws vary across the rings. Enhanced collisions in spiral density waves create blizzards of small particles, which seem to affect the brightness and color of the surrounding region. As shown by comparison of occultations at ultraviolet (UV), near-infrared (IR), mid-IR, and radio wavelengths, and by the ring spectra and color, this effect is especially significant in the outermost A-ring, the region most strongly stirred by spiral density waves.

A combination of 10–400 μm thermal emission and scattering, and 2.2 cm radiometry, suggests that ring particles probably have a low density mantle (i.e., are porous aggregates), but

might also have more dense cores. The rings' thermal emission suggests a regolith of nearly pure water ice grains of 10–100 μm size. Cassini 2.2 cm radiometry detects a fraction of a percent of non-icy material through the A-ring and B-ring, greatly improving on pre-Cassini microwave observations which could constrain the total non-icy material only to less than a few percent relative abundance. However, when combined with spiral density wave surface densities/opacities, 2.2 cm radiometry has also revealed what looks like a buried silicate-rich rubble belt in the mid C-ring; possibly the remains of the core of the ring parent.

Visual and Infrared Imaging Spectrometer (VIMS) spectra show that A-ring and B-ring composition is nearly pure water ice without any other identifiable ices such as CO, CO_2, NH_3, or CH_4, but there is a strong UV absorption making the rings unusually reddish, that varies in strength from place to place. The red color of the rings is strongest where the water ice absorption bands are deepest, suggesting that the red material resides within the icy regolith grains, and increases radially inwards at a steady rate. A third, more neutral non-icy material has a completely different radial distribution. The very low mass fraction of non-icy material (except perhaps in the C-ring rubble belt) provides our strongest constraint on the age and origin of the Rings, as discussed below. The rings' red color in the UV-visible region may be explained by fragments of carbon-bearing tholins (perhaps similar to material blanketing the surface of comet C-G as observed by Rosetta), or (some argue) by tiny iron-rich particles, embedded in the dominant water ice. Recent Cassini in situ results and remote sensing analyses, and Hubble Space Telescope (HST)-Space Telescope Imaging Spectrograph (STIS) observations, favor the organics.

New in situ data from Cosmic Dust Analyzer (CDA) and Ion and Neutral Mass Spectrometer (INMS) on the Ring-Grazing (RG) and Grand Finale (GF) orbits have greatly enriched the ring composition story. Abundant, Fe-poor silicates and organic molecules are associated with the innermost D-ring and perhaps C-ring. Evidence for organics is also found outside the rings by INMS. Reconciliation of these in situ results with remote sensing is only beginning.

Ring Variability with Time

The outer edges of the dense A-ring and B-ring vary in complex ways with both longitude and time, indicating the interference of multiple free or normal modes; possibly the result of large-scale non-axisymmetric viscous overstabilities, with the expected satellite-driven forced modes. The outer 100 km of the B-ring shows complex, fine-scale brightness variations possibly caused by these deformations. Gravitational effects of the modes might even play a role in sculpting the narrower gaps in the Cassini Division; so far found to be free of small moonlets.

Channels open and close in Saturn's F-ring strands, in response to close approaches by Prometheus, and these effects vary as the orbits of Prometheus and the F-ring mutually precess, leading to stronger and weaker gravitational interactions. Kinks and mini-jets come and go in the F-ring core, excited by small unseen objects at low relative velocities, and more dramatic jets of material lasting months are triggered by objects eccentric enough to crash through the ring at high relative velocities. These violent collisions continue because the entire F-ring region is dynamically

chaotic, mostly because of Prometheus, and for this reason the long-term stability of the F-ring core has been problematic. The F-ring has a narrow true core of large particles, as characterized best by Radio Science Subsystem (RSS), confined into discontinuous arcs and stabilized by a corotational resonance due only to Prometheus. The fine dust seen in images and stellar occultations is a tiny fraction of the F-ring total mass. Clump activity has varied dramatically between Voyager and Cassini.

Vertical ripples or warps covering the inner part of the rings, which have changed even over the duration of the mission, suggest that Saturn's D-ring and inner C-ring were tipped relative to its equator several times over the last millennium, and as recently as a few decades ago. Impacts by rubble streams produced by disrupted objects are the most likely cause. Several impacts by individual m-size projectiles have actually been seen and catalogued.

Diffuse Rings Dominated by Tiny Dust Grains are Affected by Sunlight and Magnetic Fields

The source of the E-ring particles has been confirmed as the south polar jets of Enceladus (see the Icy Satellites chapter). Several new arcs and ringlets are associated with erosion of small embedded moons. The E-ring and other diffuse rings and ringlets (such as those in the Encke gap) are affected by sunlight and electromagnetic forces as well as by gravity, and thus show seasonal variations in their structure. Some diffuse rings, notably the D-ring and the faint material between the A-ring and F-ring, are modulated by azimuthal variations in Saturn's magnetic field.

The duration and behavior of the spokes Voyager discovered in the B-ring have been further constrained, though their ultimate cause or trigger remains unknown. Cassini found that they seasonally appear and disappear, probably due to variable photo-charging of the main ring layer, and their temporal periodicities match best that of the northern hemisphere Saturn Kilometric Radiation (SKR) during the 2008–2009 timeframe, though contributions from the southern SKR source could not be ruled out. Any association with the Saturn Electrostatic Discharges (SEDs) was ruled out.

Ring Mass

Voyager-era estimates of the ring mass were roughly 0.7–0.8 Mimas masses. It was since suggested that the breakdown of the ring layer into opaque clumps (the self-gravity wakes), separated by nearly empty gaps, could allow a lot of mass to be hidden in the clumps. Modeling of dozens of spiral density and bending waves over Cassini’s first decade had constrained the mass of the A-ring, C-ring, and inner B-ring, so any hidden mass had to reside in the densest parts of the B-ring. In the Grand Finale orbits, the Cassini RSS team tracked the spacecraft to constrain the ring mass by its perturbation on Cassini's orbit, and concluded that the ring mass is not very different from, and likely lower than, our Voyager-era expectations.

Origin and Age of the Rings

The strongest constraint on ring age is provided by the gradual darkening and restructuring of the rings with time by infalling meteoroids. Inferring the actual ring age requires knowledge of the current mass fraction in non-icy pollutant, as well as both the incoming meteoroid mass flux and the total mass of the rings. The Cassini CDA experiment has determined, cumulatively over the entire mission, the infalling meteoroid mass flux and dynamical population. The mass flux far from the planet is not too different from pre-Cassini estimates. However, the dynamical population is like that of Kuiper Belt objects, so has a lower encounter velocity and is more strongly focused by Saturn's gravity than thought previously. This means that the flux of meteoritic material actually hitting the rings is probably even larger than previously thought. Combining the ring mass with the CDA-determined meteoroid mass flux, and estimates of non-icy pollution currently in the rings, leads to a ring exposure age of 100–200 million years, perhaps even a little younger than Voyager-era young-ring scenarios.

Combining the ring mass with the CDA-determined meteoroid mass flux, and estimates of non-icy pollution currently in the rings, leads to a ring exposure age of 100–200 million years … .

The associated puzzles of “Why is Saturn the only giant planet with rings?” and “Is the ring system young?” have been, if not yet explained, at least illuminated by an emerging hypothesis involving a closely-coupled tidal evolution of the mid-sized icy moons leading to a Saturn-specific dynamical instability of the inner satellite system, with possible disruptions and reaccretion, on the order of 100 million years ago. Constraints from satellite surface geology will need to be folded in to evaluate the plausibility of the scenario.

Overall Assessment of Ring and Dust Science

All key science objectives listed in the Announcement of Opportunity (AO) and Solstice Traceability Matrix (TM) were successfully accomplished over the course of the Cassini mission. In addition, a number of new science objectives were formulated and addressed along the way either in response to unexpected results or capitalizing on observational opportunities (some not originally envisioned, and some in greater numbers than envisioned). When the mission was approved, the AO Objectives reflected a 4-year baseline tour with only 59 orbits, allowing at most 16 Radio occultations, and of course did not incorporate the RG or GF observing geometries.

By the end of the mission, even the four-year baseline tour had been optimized to include 74 (generally shorter) orbits, wasting less time far from the planet, and had also been extended by nine years, tripling the total time baseline for observations relative to the AO. The final tour lasted 13 years, sampling three different seasons and reaching northern summer solstice (the maximum opening angle of the rings as seen from Earth and the Sun) which allowed the radio occultations to better penetrate the optically thickest parts of the B-ring. The mission included 282 orbits capturing

many new combinations of illumination and viewing angles important for imaging—VIMS and Ultraviolet Imaging Spectrograph (UVIS) spectral reflectance mapping, and Composite Infrared Spectrometer (CIRS) thermal mapping. Datasets returned included 135 ring radio occultations (each at 3 wavelengths), 170,000 ring images (many at < 1 km/pxl), over 200 UV stellar occultations, 170 near-IR stellar occultations, 30 solar occultations, and even a few occultations at thermal, mid-IR wavelengths.

The stellar occultations made use of dozens of stars with different elevation angle relative to the rings; low-optical depth rings are best studied by low-elevation stars, and high optical depth rings by high-elevation stars. In addition, several complete 2.2 cm microwave emission maps or radial scan combinations were obtained in different geometries and resolutions, and three active radar backscattering scans were obtained in the RG and GF orbits when the spacecraft was close enough to overcome the fourth-power dependence of radar sensitivity on distance. Moreover, the RG and GF orbits provided in situ ring particle composition sampling opportunities for CDA, INMS, and Magnetospheric Imaging Instrument (MIMI) that were not part of the AO plan, and enabled direct determination of the ring mass from spacecraft tracking of the RSS signal. VIMS stellar occultations were not even envisioned in the AO, but were added after selection of the instruments. This new stellar occultation capability provided a very useful wavelength difference compared to UVIS, and an entirely different angular distribution of sources on the sky. Using the Radar as a passive pencil-beam microwave ring brightness mapper, or to obtain active radar backscattering radial profiles from the rings were also not part of the original plan.

The overall science data volume return of Cassini was more than 100 times that of Voyager in the instruments they both carried (not to mention the roughly 200 times longer time baseline at interesting resolution) and the numerous unique new remote and in situ observations provided by Cassini. There is no question that the science return of Cassini vastly exceeded the expectations as described in the AO.

Summary of Key Open Questions

Overall, Cassini has answered many of the questions raised by Voyager, raised new ones, and leaves us with a largely untapped reservoir of data with which to answer. These questions and others are discussed in more detail in the section entitled Unsolved Problems Suitable for Ongoing Research and Future Missions.

The overall ring mass is known now, but with low precision and no radial resolution. Is the B-ring mass uniformly distributed according to optical depth, or is it even more strongly concentrated in the still nearly opaque central regions? Does the C-ring contain a rocky rubble belt? Future missions with tracking capability and multiple close passes will be needed, and should be planned to also provide a better understanding of why Saturn’s own interior is so different from Jupiter’s.

Most ring structure is still a puzzle. The irregular structure blanketing the entire B-ring, with lengthscales narrowly concentrated near 80 km in the inner B-ring, but covering a wider range of scales from the resolution limit to several hundred km in the mid-and outer B-ring, remains a mystery. In the inner-mid B-ring there are very sharp optical-depth jumps (but not to empty space) that are barely explored and remain unexplained.

The entire ensemble of so-called plateaus in the outer C-ring, symmetrically placed around the Maxwell gap in the C-ring, which is known to be caused by structure in Saturn's interior, and incorporating other empty gaps is not understood. The plateaus also contain a unique kind of streaky microstructure not seen elsewhere, which was only seen in a limited way during the final orbits.

There are several significant features (A-ring inner edge, C-ring plateaus), which have sharp well-defined boundaries, that are defined only by changes in the particle size distribution across which the surface mass density does not change. This structural control of particle size distribution, or vice versa, is not understood.

The mere presence of the Cassini Division is an unsolved problem, although it is plausible that a strong density wave driven by the 2:1 resonance with Mimas had a role in creating it when the rings were more massive and material filled the region. The apparent lack of moonlets capable of clearing the 13 gaps in the Cassini Division and C-ring, especially the 5–6 that have no embedded ringlets[1], is a puzzle. A clue may be found in the apparently non-random spacings of the edges of the Cassini Division bands and gaps, perhaps somehow manifesting gravitational influence of the B-ring outer edge.

The unusually red color of the A-ring and B-ring, which are surely more than 95% water ice and probably more than 99%, seems to be due to organic material based on a combination of remote and in situ measurements. However, composition varies from place to place and on a range of scales. Models capable of interpreting color and spectral data quantitatively in terms of underlying composition are inadequate and need improvement. The hint of a rubble belt of non-icy material buried in the mid-C-ring is intriguing, but remote observations are ambiguous and the analysis of in situ observations is only getting underway. Whether or not organics explain the similarity, but relatively weak, UV absorption seen in most icy moons is not yet known—the dark side of Iapetus has been fit by carbon, nano-iron, and metal oxides. Why is the G-ring parent body, so close to the icy main rings, so dark?

Are the A-ring (and B-ring) propeller objects the shards left over from the ring parent? Why do the dozen or so giant propellers found only outside of the Encke gap wander in semi-major axis, and what (if any) patterns are present in the evolution? Are there cyclic, self-limiting processes of growth and disruption of sub-km sized objects in the outer A-ring (and B-ring)? The F-ring core is stabilized by Prometheus, but what causes its uniformly precessing eccentricity? Do relatively large

[1] Cassini Division gaps with ringlets: Huygens, Herschel, Laplace; and without ringlets: Russell, Jeffreys, Kuiper, Bessel, Barnard. C-ring gaps with ringlets: G1, Colombo, Maxwell, Bond; and without ringlets: Dawes.

objects form in regions compressed by Prometheus and go on to crash through the core, creating clumps and strands?

The rings seem to be much younger than the solar system based on nominal results to date, and there is one encouraging hypothesis (a 200-million year ago system-wide instability) providing the proper context. However, questions remain including consistency (or lack of it) of the observed icy moon cratering distributions with reaccretion of most of the inner icy moons on that same timescale.

KEY OBJECTIVES OF THE RINGS WORKING GROUP

The original ring objectives from the AO, and those added for the extended Cassini Solstice Mission, are given in Table RINGS-1. We assess Cassini as fully successful, at least in all regards. It is emphasized that in almost all cases there has been far more data obtained, reduced, and archived than the teams have had time to analyze and interpret.

Rings AO Objectives

- **Ring Structure and Dynamics (R_AO1)** – Study configuration of the rings and dynamical processes (gravitational, viscous, erosional, and electromagnetic) responsible for ring structure.
- **Ring Particle Composition and Size (R_AO2)** – Map composition and size distribution of ring material.
- **Ring-Satellite Interaction (R_AO3)** – Investigate interrelation of rings and satellites, including embedded satellites.
- **Dust and Meteoroid Distribution (R_AO4)** – Determine dust and meteoroid distribution both in the vicinity of the rings and in interplanetary space.
- **Ring Magnetosphere-Ionosphere Interactions (R_AO5)** – Study interactions between the rings and Saturn's magnetosphere, ionosphere, and atmosphere.

Rings CSM Traceability Matrix Objectives

- **Changing Rings (RC1a)** – Determine the seasonal variation of key ring properties and the microscale properties of ring structure, by observing at the seasonally maximum opening angle of the rings near Solstice.
- **Ring Temporal Variability (RC1b)** – Determine the temporal variability of ring structure on all timescales up to decadal for regions including Encke gap, D-ring, F-ring, and ring edges by substantially increasing the cadence and time baseline of observations.

- **F-ring (RC2a)** – Focus on F-ring structure, and distribution of associated moonlets or clumps, as sparse observations show clumps, arcs, and possibly transient objects appearing and disappearing.
- **Ring Age and Origin (RN1a)** – Constrain the origin and age of the rings by direct determination of the ring mass, and of the composition of ring ejecta trapped on field lines.
- **Ringmoons – Composition (RN1b)** – Determine the composition of the close-in ringmoons as targets of opportunity.
- **Ring Structure – High Resolution and Composition (RN1c)** – Determine structural and compositional variations at high resolution across selected ring features of greatest interest, using remote and in situ observations.
- **Ring Microstructure (RN2a)** – Conduct in-depth studies of ring microstructure such as self-gravity wakes, which permeate the rings.
- **New Ring Structures (RN2b)** – Perform focused studies of the evolution of newly discovered propeller objects.

Table RINGS-1. RWG Science Assessment.

Fully/Mostly Accomplished: **Partially Accomplished:** **Not Accomplished:**

RWG Science Objectives	AO and TM Science Objectives	RWG Science Assessment	Comments (if yellow, partially fulfilled)
Ring Structure and Dynamics	R_AO1		
Ring Particle Composition and Size	R_AO2		
Ring-Satellite Interactions	R_AO3		
Dust and Meteoroid Distribution	R_AO4		
Ring-Magnetosphere-Ionosphere Interactions	R_AO5		
Changing Rings	RC1a		
Ring Temporal Variability	RC1b		
F-ring	RC2a		
Ring Age and Origin	RN1a		
Ring Composition - ringmoons	RN1b		
Ring Structure - high resolution and composition	RN1c		
Ring Microstructure	RN2a		
New Ring Structures	RN2b		

These objectives are discussed below in more detail.

RWG SCIENCE RESULTS

Prime Mission (AO) Original Objectives (Highest, Top-level Results)

Ring structure and dynamics (R_AO1)

Studies configuration of the rings and dynamical processes (gravitational, viscous, erosional, and electromagnetic) responsible for ring structure.

This objective, perhaps the broadest and deepest, was satisfied beyond our initial expectations. Stellar and radio occultations are the most powerful tool for exploring structure at high resolution. During initial planning sessions, the UVIS team was considering dozens of stellar occultations as an optimistic goal, and ended up with over 200, including the novel turnaround occultations in which the line of sight to the star moves parallel to the particle orbits, at very low velocity, allowing azimuthal structure to be determined with high resolution at perhaps a dozen radii and structure on the scale of a ring thickness to be addressed statistically. Moreover, VIMS developed a stellar occultation capability of their own that was not part of the original plan, and went on to produce almost 200 occultations of their own in geometries that were independent of and complementary to those available to UVIS, because they observed a different set of stars. All these stellar occultations reside on the Rings Planetary Data System (PDS) node in 1 and 10 km resolution format. In addition, RSS conducted 135 occultations at three radio wavelengths (0.94, 3.6, and 13 cm), which all reside on the Rings PDS node in 1 and 10 km resolution format, and for which further processing (by diffraction correction) can generally provide 100 m or even better radial resolution. More analysis of these data will provide additional surprises and constraints. Review chapters by Colwell et al. [2009] and Cuzzi et al. [2018] cover the major advances regarding observed ring structure, Schmidt et al. [2009] review advances in the theory of dense ring structure, and Horanyi et al. [2009] review advances in the theory of electromagnetic influences (most significant on tiny dust grains).

CONFIGURATION OF THE RINGS

The Grand Structure of the rings (Figure RINGS-1) was elucidated for the first time by Voyager, reviewed by Orton et al. [2009] and Colwell et al. [2009]. In this section we will discuss the so-called main rings (A-ring, B-ring, and C-ring) and the Cassini Division, all of which have optical depth > ~0.1 (Figure RINGS-1). The A-ring is the best understood by Voyager-era theory; blanketed by spiral density and bending waves from nearby moons, with embedded moonlets that carve empty gaps by the process of gravitational shepherding, and a ubiquitous non-axisymmetric microstructure having scales comparable to the ring thickness due to local gravitational instabilities. All of these structural properties have been closely observed by Cassini, in greater numbers, with greater radial coverage, in more geometries, in finer detail, and at better sensitivity than ever before. The B-ring and C-ring contain a few of these well-understood features too, but are overwhelmingly dominated by structure on all scales that is simply not understood at present (see

section entitled Electromagnetic and Radiative Processes). The so-called diffuse rings (D-ring, E-ring, and G-ring) and dusty rings associated with various moonlets, have optical depths much less than unity and are a separate class of structure discussed in sections entitled Dust and Meteoroid Distribution, and Ring Magnetosphere-Ionosphere Interactions. The narrow, kinky F-ring lying just outside the A-ring has captured a niche of its own and is discussed mostly in the section entitled F-ring.

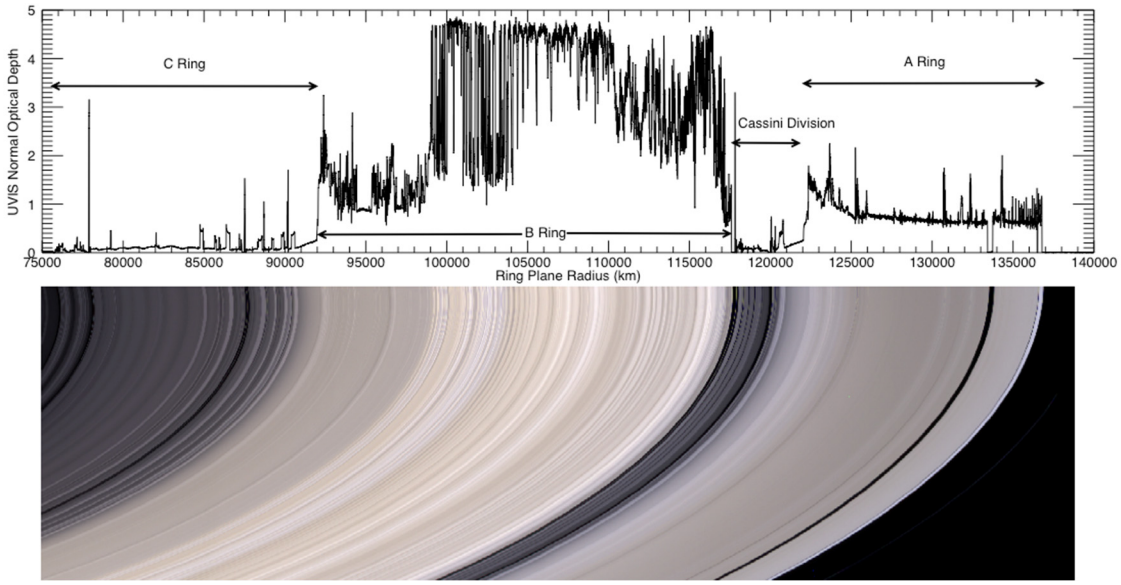

Figure RINGS-1: Main rings of Saturn. The image is registered along its top edge with a radial profile of the ring optical depth from a Cassini UVIS stellar occultation. The optical depth (usually denoted τ) is the vertical integral through the ring layer of the particle number density times its cross-sectional area, times extinction efficiency (for the plot above, the efficiency is unity). The B-ring (especially its central part) has the highest optical depth, but the highest values shown are just noise limits. Unlabeled regions mentioned in the following text include the series of plateaus in the outer C-ring, centered on the Maxwell gap near 87500 km, which contains an elliptical ringlet. The Encke gap is visible in the outer A-ring, around 133600 km. The narrow, stranded F-ring is just off the figure at right. Figure from Colwell et al. [2009].

The local ring thickness was a perennial topic of discussion before Voyager and measurements of kilometers were reported (now known to be better explained by vertical corrugations and/or the inclined F-ring). The single Voyager stellar and Radio occultations showed that ring edges were so sharp that the local thickness (at least at edges) could be no more than tens of meters. Cassini's hundreds of stellar and radio occultations have extended this knowledge to nearly all locations except the opaque central B-ring [Colwell et al. 2006, 2009; Hedman et al. 2007b]; see also Tiscareno et al. [2007]. This small vertical thickness means that the rings are not the many particle thick classical layer envisioned even in the Voyager era, and have a moderate volume density of 0.01–0.1 [Salo and French 2010] or even larger. There are implications of high volume density for ring viscosity (see section entitled Viscous Processes). Another indication of volume density (and thus local dynamics) comes from mutual shadowing. Visual brightness observations have long shown a sharp opposition peak that was traditionally interpreted in terms

of shadowing in a many-particle-thick layer; however, dynamical constraints and the increased recognition of the importance of coherent backscattering in grainy particle regoliths (see Cuzzi et al. [2009] for a review) complicate this interpretation [Salo and French 2010]. CIRS observations show a much broader phase effect in particle temperatures; however, that is plausibly shadowing-related (unlikely to be contaminated by coherent backscattering) and consistent with non-classical rings [Altobelli et al. 2007, 2009; Reffet et al. 2015; Morishima et al. 2017; Deau et al. 2019]. These thermal studies lead to midplane particle volume densities as large as 0.3–0.4 in the B-ring. Finally, analysis of 2.2 cm radiometry is best fit by modeling closely packed cm-m size particles in the near-field scattering regime [Zhang et al. 2017b, 2019].

There has been a start taken on modeling of imaging observations of the rings over a wide range of geometries, with an emphasis on unraveling opposition effects of different kinds using classical radiative transfer models [Deau et al. 2013, 2018; Deau 2015]. However, interpreting UV, visual, and near-IR observations using realistic models of closely packed particles with rough shadowed surfaces, which might provide more insight into radial variations of local particle volume density and thus local dynamics, remains in its infancy (see Porco et al. [2008] for the only example).

Gravitational processes (self-gravity wakes, spiral waves, and shepherding torques)

Probably the longest-known and most widespread gravitational process leads to the self-gravity wakes, caused by local, transient, incipient gravitational instabilities which are stretched into trailing clumps of scale comparable to the ring thickness (indeed defining the ring thickness) by Keplerian shear, keeping the ring in a constant state of frustrated satellite formation [Orton et al. 2009; Schmidt et al. 2009; Colwell et al. 2009]. Imaging observations have characterized the effect in the A-ring, using the azimuthal brightness asymmetry known for decades, but finding the particle collisional elasticity to be smaller than thought; indicating either a rough surface or a porous regolith [Porco et al. 2008]. The effect has also been observed and modeled in the thermal IR [Leyrat et al. 2008; Ferrari et al. 2009; Morishima et al. 2014]—see also section entitled Extended Mission (CSM) Objectives, Section 3.2 Instrument Science Results chapter entitled CIRS, and Spilker et al. [2018]. A CAT-scan technique of characterizing the horizontal and vertical scales of these structures as well as their angle relative to the orbit direction was developed based on stellar occultations from a variety of slant directions. These models of the dense gravitational wakes as optically thick granola bars or elliptical cylinders [Colwell et al. 2006, 2007; Hedman et al. 2007a; Nicholson and Hedman 2010] (see also Colwell et al. [2009] for a review) provide valuable mean values of the orientation, width, height, and separation of dense clumps for use in models of ring brightness. The pitch angle of the wakes, relative to the orbit direction, decreases radially inwards as differential rotation becomes stronger.

Perhaps the most obvious, beautiful, and useful gravitational ring structures are spiral density and bending waves at isolated satellite resonances. These striking features share the physics of the arms of spiral galaxies, but are tightly wrapped like watchsprings [Shu 1984; Schmidt et al.

2009]. They propagate away from their driving resonance with a decreasing wavelength—density waves move outwards and bending waves inwards. The wavelength itself is diagnostic of the underlying surface mass density on scales smaller than a wavelength. Thus, spiral density wave measurements provide our best idea of the radial profile of mass density, in regions where they are found. This property is extremely important, because the almost ubiquitous clumping due to self-gravity wakes breaks the rings into a set of opaque regions separated by nearly empty gaps, for which the optical depth (see Figure RINGS-1) is of questionable basic value.

For this reason, Robbins et al. [2010] suggested that inferences of ring surface mass density from a combination of observed optical depth and particle size distribution might greatly underestimate the ring mass. This reasoning led to a debate as to whether the ring mass could be much larger than Voyager-era estimates, because most of the B-ring (which contains most of the mass) is unsampled by diagnostic density and bending waves, with implications for ring age (see section entitled Ring Age and Origin). The debate tilted in favor of low mass when Hedman and Nicholson [2016] succeeded in obtaining some B-ring density wave measurements despite the noisy background, and has now been definitively resolved in that direction by the RSS total mass measurements based on gravitational tracking (see section entitled Determination of Ring Mass). The RSS gravity measurements have little or no radial resolution, but used A-ring and C-ring masses as determined from these waves [Colwell et al. 2009; Tiscareno et al. 2013] and assumed the remainder of the measured mass to be that of the B-ring. They do suggest, though, that the surface mass densities obtained from spiral density waves are insensitive to the suggested clumping difficulty.

One important surprise from measuring surface mass density is that several important structural features, long seen in images and occultations, actually manifest as distinct structures not because they have higher local mass density as was usually assumed, but because their local particle size distribution changes in a dramatic way making them more opaque than their surroundings without much change in their underlying surface mass density. This happens because the surface-to-mass ratio of a particle, or of a distribution of particles, increases as particle size decreases. The effect is seen at the inner edge of the A-ring and all of the C-ring plateaus—sharp optical depth jumps are seen where there is at most a gradual change in surface mass density [Tiscareno et al. 2007, 2013a; Tiscareno and Harris 2018]. Baillié et al. [2011] and Hedman and Nicholson [2014] show surface mass densities for the plateaus and background C-ring, and Colwell et al. [2018] show drops in effective particle size in the plateaus, consistent with a small change in surface mass density despite a large increase in optical depth. This important phenomenon of locally abrupt changes in the particle size distribution is not currently understood, but is clearly of central importance to understanding the formation of these structures.

Another important clue from density and bending waves is obtained from sparse sampling of the C-ring, showing that the surface mass density radial profile differs from the optical depth profile in a fashion most easily explained if the local particles (whose sizes are well known from RSS occultations) are several times more dense in the central C-ring than elsewhere in it; possibly hinting at buried rocks in unusually high abundance and perhaps to a hidden rocky rubble belt [Zhang et al. 2017a], see also section entitled Ring Particle Composition and Size. Sampling of the

B-ring is even sparser, but generally points to surface mass densities somewhat lower than previously thought [Hedman and Nicholson 2016; Tiscareno and Harris 2018].

An interdisciplinary bonus was the confirmation of the prediction by Marley et al. [1987, 1989]; Marley [1990]; and Marley and Porco [1993] that density fluctuations in Saturn's interior produced by planetary scale acoustic oscillations (modes) can drive spiral density and bending waves similar to those driven by an external satellite. A number of unidentified waves had been noted by Rosen et al. [1991] in Voyager RSS occultation data. Marley and Porco [1993] suggested several specific associations between predicted resonance locations and these Rosen waves. They also suggested that the strongest predicted (two-lobed, or m = 2) planetary interior resonance might be associated with the unexplained Maxwell gap, where there was an unexplained eccentric (m = 1) ringlet.

Cassini, along with subsequent improvements in the Saturn interior model, have confirmed the Marley and Porco [1993] predictions, putting the study of ring seismology on firm ground and finding in the process other features likely due to variations in internal structure not accounted for in the simple 1993 interior model. The great advantage of Cassini data is multiplicity and accuracy of occultation measurements, allowing both the number of spiral arms and the pattern speed of the waves to be determined unambiguously, and thus finer associations to be made with theoretical predictions [Hedman and Nicholson 2013, 2014; Marley 2014; French et al. 2019; Mankovich et al. 2019; Hedman et al. 2019]. Initially, some Rosen waves, and newly discovered ones [Baillié et al. 2011] were found to have the same value of m, something not predicted by Marley and Porco [1993]. However, Fuller et al. [2016] showed that allowing a compositionally-stratified layer deep inside Saturn could explain these multiplicities because such a gradual density transition would allow different types of modes to mix inside the planet. Next, a two-armed spiral density wave was discovered within the (m = 1) Maxwell gap ringlet [French et al. 2016b] validating the association of the gap with the strongest (m = 2) mode as predicted by Marley and Porco [1993]. Finally, Mankovich et al. [2019] have recently shown that slightly changing the interior rotation period of Saturn allows the detailed predictions of Marley and Porco [1993] to be very well matched across 16 sets of waves over a wide range of relative strengths, with the strongest perturbation opening the Maxwell gap. In fact, this excellent agreement provides the best constraint yet on the deep interior rotation period of Saturn—a fundamental property that has been elusive because of the almost complete lack of magnetic field azimuthal asymmetry [Dougherty et al. 2018] (see also Section 3.1 Discipline Science Results chapter entitled MAPS). In addition, a new class of density waves has been found in the B-ring and A-ring; waves that are driven by density structures of unknown origin, fixed to the body of Saturn [El Moutamid et al. 2016a, 2016b]. Surprisingly, some of these wave features are actually seen to drift radially inwards in the rings, indicating temporal changes in Saturn's interior structure on a decade timescale [Hedman et al. 2017, 2018b; Hedman and Nicholson 2014]. Therefore, ring properties and physics have led to three new important insights into the deep interior of Saturn. See section entitled Ring-Satellite Interaction for more

… a new class of density waves has been found in the B-ring and A-ring—waves that are driven by density structures of unknown origin, fixed to the body of Saturn .

discussion of interactions between satellites and moonlets with the rings, which are mostly gravitational.

VISCOUS PROCESSES

Because of their innumerable particles in a constant state of gentle collisions, the rings act like a gas or fluid and obey the equations of fluid dynamics with local pressure and viscosity. They spread radially due to viscosity, an important aspect of their evolution that combines with other angular momentum and mass transport processes like shepherding, wave torques, and ballistic transport of meteoroid ejecta. The theory of spiral density waves is mature enough that the rate at which their amplitude damps as they propagate can be used to constrain the local ring viscosity [Schmidt et al. 2009, 2016; Colwell et al. 2009].

A second kind of so-called ring microstructure, called a viscous overstability, occurs on scales of the ring vertical thickness and is partly driven by viscosity [Schmidt et al. 2009]. In this effect, a stable (non-growing) radial oscillation can develop that comprises axisymmetric, alternating ringlets of high and low density that pulsate on the orbital timescale. These structures are aligned with the orbital direction and were first distinguished by subtle Doppler effects in off-axis scattering during Cassini RSS occultations [Thomson et al. 2007], but have also been detected using statistical analysis of stellar occultations [Colwell et al. 2009; Hedman et al. 2014a]. They are widespread across the rings and generally found with the expected lengthscales (comparable to a ring thickness) in regions where the optical depth is moderate to high. Self-gravity plays only a small role in these structures.

Viscous overstabilities can take on non-axisymmetric forms as well. For example, in a densely packed ring, collective behaviors akin to those seen in granular flow can occur and viscous stress can actually decrease the damping between adjacent orbital motions effectively by locking particles and their orbits together. Where there is also the opportunity for double reflection of spiral density waves, as within a narrow isolated ring bounded by sharp edges, or a so-called resonant cavity, they can become amplified [Borderies et al. 1985; Hedman and Nicholson 2019] generating low-order (m = 1, 2, 3, etc.) modes. The m = 1 and m = 2 structure of the narrow sharp-edged rings of Saturn and Uranus may be explained in this way. For instance, the Maxwell ringlet exhibits an m = 2 spiral density wave forced by an m = 2 acoustic mode within Saturn (see section entitled Gravitational Process), but attains an m = 1 overall structure. However, Cassini discovered large-scale, unforced, or free modes with m = 1, 2 and 3 in the outer portion of the B-ring, in addition to the resonant m = 2 mode forced by Mimas at the B-ring's edge [Spitale and Porco 2010], see also section entitled Ring Temporal Variability). The large-amplitude m = 1 mode, in particular, would damp quickly without both the overstabilizing viscous effects described above and the amplification accompanying multiple reflections within the resonant cavity formed by the B-ring outer edge and the mode's own resonant radius some 250 km inwards. The discovery of these unforced modes is the first indication of substantial wave amplification on large scales, in broad rings. These modes may have applications to other celestial disks, such as protoplanetary nebulae [Laughlin et al. 1997] and spiral galaxies.

Viscosity and pressure due to ring particle collisions determines the ability of ring particles to move from one face of the rings (lit face) to the other (unlit) face, and models have been applied to CIRS thermal observations to address this constraint [Flandes et al. 2010; Pilorz et al. 2015; Morishima et al. 2016]. Another manifestation of particle collisions would be to pack surface regoliths to varying degrees, depending on local dynamics. CIRS tried to measure radial variations in particle thermal inertia (higher for more packed particle surfaces), but the complexities of the models, the complications due to small and/or rapidly rotating particles, and the incompleteness of the observing phase space has so far precluded more than a basic determination that the ring particles look like other frosty outer solar system objects. Section 3.2 Instrument Science Results chapter entitled CIRS describes how models of ring thermal observations can address these and other issues in more detail.

Erosional processes

Pollution of the mostly icy ring material by meteoroid bombardment, erosion of ring particles into impact ejecta, and restructuring of the rings by Ballistic Transport of the ejecta, were first suggested and discussed in the pre-Cassini era—see Durisen et al. [1989, 1992]; Cuzzi and Estrada [1998]; and see also the section entitled Ring Origin and Age for more discussion. The process is a little subtle and counterintuitive—see more recent work in Charnoz et al. [2009] and Estrada et al. [2015]. Extrinsic meteoroids hit the rings at tens of km/s, not only depositing their substantial amount of non-icy material, but ejecting chips of the target ring particle at 1–100 m/s. These chips go off on orbits that re-impact the rings where they become part of a new ring particle. Exchanges of losses and gains of mass and angular momentum can result in significant radial restructuring of the ring surface mass density over a time short compared to the age of the Solar System, given what we now understand about the meteoroid flux—see section entitled Dust and Meteoroid Distribution.

Signatures of this process can be found both in ring structure and ring composition. To date, intriguing possible correspondences to observed structure have been seen (amongst them the abrupt inner edges of the A-ring and B-ring and the odd linear ramps inward of them, and the 80 km scale irregular structure in the inner B-ring and inner A-ring) and a good match is provided to the smooth compositional profile that accompanies the abrupt B-ring–C-ring boundary. These independent structural and compositional properties suggest a young ring age of a few hundred million years, extending the simpler pollution argument relying on deposition of non-icy material alone, see section entitled Ring Particle Composition and Size, but the models have many parameters and face new challenges from new discoveries of several kinds (see section entitled Non-Saturn-System Science Results).

Electromagnetic and radiative processes

Particles in the space environment tend to attain a maximum charge that is only large enough to affect the dynamics of tiny (at most 10 micron size) grains. An entire branch of ring dynamics has to do with resonances involving forcing of tiny charged grains by the periodically fluctuating

planetary magnetic field; so-called Lorentz Resonances [Burns et al. 1985; Schaffer and Burns 1987], see also Horanyi et al. [2009] and Hedman et al. [2018a] for reviews of these and other electrodynamical effects. The most obvious places where these processes will be important is in the diffuse rings, such as the D-ring, E-ring, and G-ring, which are known to be most easily delineated by their tiny particles [Hedman et al. 2009a, 2018a; Chancia et al. 2019]. The E-ring shows the most clear influences, including its preference for a near-monodispersion of particle size at around one micron radius, a radial profile with a local minimum in vertical thickness at the location of Enceladus, and 3-D variations that correlate with the orientation relative to the Sun [Hedman et al. 2012; Ye et al. 2016]. It is now known that the E-ring is the frosty breath of Enceladus, and analyses of ISS images have clarified how it is fed in some detail [Mitchell et al. 2015].

A second ring phenomenon widely thought to be connected to electromagnetic forces is the flickering of shadowy spokes across the A-ring and B-ring, discovered by Voyager, see reviews by Orton et al. [2009] and Horanyi et al. [2009]. Various periodicities in the Voyager spoke occurrence rates, rotation rates at spoke boundaries, and the angular and spectral scattering properties of spoke regions have implicated electromagnetic effects acting on tiny grains; with sizes most recently shown by D'Aversa et al. [2010]. The tiny grains are probably released sporadically from ring particle surfaces somehow, perhaps by m-size particle impacts, energy beamed from the planet, or magnetic field/plasma instabilities near the ring, reviewed by Horanyi et al. [2009]. Earth-based observations also contributed to this understanding [McGhee et al. 2005]. Surprisingly to most of the Cassini team, spokes were invisible on approach and for the first year or more of the mission, and initially seen only weakly in late 2005 [Mitchell et al. 2006]. This observation supported an idea first suggested by Nitter et al. [1998] that seasonal changes in photocharging by the Sun were responsible. In this theory, dust is constantly being lofted out of the ring plane by impacts, but when the solar elevation is high, electrons are photosputtered out of the dense main ring layer causing the main rings to be positively charged while embedded in a vertically extended negatively charged electron plasma. Grains ejected from the rings become negatively charged in this plasma and are swept immediately back into the rings by the strong vertical electric field. The process is like an electrostatic dust precipitator in an industrial smokestack. The theory predicted that at a certain low elevation angle, the electrostatic precipitation would cease and spokes would reappear (Voyager 1 and 2 flybys were both at a time of low solar elevation) and indeed their disappearance again a year or so after equinox proved this to be the case. During the brief time spokes were abundant (roughly 2009–2011), detailed studies of their morphology [Mitchell et al. 2013] showed that the spokes had extended active growth times, both radially and azimuthally, and that their activity level was most likely associated with one of the SKR periods, but maximizes at a different longitude in that system than found by Voyager.

Finally, certain dusty ringlets in various otherwise empty gaps in the rings suggest evidence for electromagnetic or even solar radiative control on their predominantly micron-sized grains. The very obvious dusty, eccentric so-called "charming" ringlet in the outermost Cassini Division gap, that was not very noticeable during either Voyager encounter, always points its apoapse towards the Sun due to radiation pressure [Hedman et al. 2010a]. Several dusty, clumpy ringlets in the Encke gap have similar properties [Hedman et al. 2013b]. In general, one would expect that these tiny grains are constantly resupplied by generally unseen strands or clumps of macroscopic

particles with comparably low optical depths, but such a belt of more massive particles would not be influenced by electromagnetic or radiative forces.

Ring particle composition and size (R_AO2)

Maps composition and size distribution of ring material.

As described in more detail in the section entitled Ring Origin and Age, understanding the non-icy mass fraction in the rings is critical, as it provides perhaps the strongest constraint on the age and origin of the rings.

COMPOSITION (REMOTE SENSING)

The goal was to determine the composition of the ring material with the best possible radial resolution across the main rings. Spectral observations at UV, visual, and near-IR (NIR) wavelengths are generally insensitive to ring particle size because the ring particles were known to be much larger than these wavelengths from groundbased and Voyager observations. Known ring structure is on scales of 100–300 km, so observations needed to be planned to enable VIMS, UVIS and CIRS; all having much lower resolution than ISS, to resolve these scales. Longer observation times allowing deeper integrations were possible at greater distances, and high SNR spectra of broad segments of the A-ring, B-ring, and C-ring were also obtained. As time went on, we learned more about the observations and about the rings. For instance, Saturnshine was found to contribute organic-looking spectral features in certain geometries (ring longitudes between 120–240° solar hour angles as observed from high phase angles, for instance). The VIMS and UVIS calibration pipelines evolved and improved as the mission went on, and data analyzed and published early in the mission might still profit from reanalysis. ISS, while having much higher resolution and typically obtaining 3–5 km/pxl in extended color sequences, has very limited spectral resolution. In-depth ISS sequences were planned, but only one lit face observation in all 15 filters was obtained in Prime Mission, which was corrupted, so extensive and redundant follow-up was planned for the extended or Cassini Solstice Mission (CSM), over a range of illumination and viewing geometries (see section entitled High-resolution Ring Structure and Composition). Regional and local radial variations in color and spectra were seen by UVIS, ISS, and VIMS, greatly expanding geometrical and wavelength coverage to a depth of data that has yet to be plumbed. However, going from observed reflectivity (or I/F, the ratio of observed intensity to that of a colocated Lambert surface) to quantitative constraints on ring particle composition is a somewhat imperfect modeling step, involving the poorly understood way closely spaced particles with rough, grainy regoliths scatter light (see section entitled Non-Saturn System Science Results).

Allowing for most of these complexities, VIMS spectral data has been especially powerful in connecting the abundance and regolith grain size of water ice with the relative abundance of other materials. Early in the mission, Nicholson et al. [2008] found, and subsequently Hedman et al. [2013a] showed in more detail, that the redness of the main rings correlated very well with the water ice band depth suggesting that the UV absorber was spatially colocated with water ice, most likely

as tiny submicron or smaller size inclusions within the water ice regolith grains (new in situ observations may have even detected these tiny few-nm-size inclusions directly, see section entitled Composition of Rings From Ring Ejecta). Detailed studies of radial variation of color and spectra are reviewed by Cuzzi et al. [2009, 2018b, and references therein]. Regarding the actual nature of the UV absorber, a lively debate has continued for a decade as to whether the rings' redness can be better explained by good old-fashioned rust or other metal oxides, as on Mars, or by large organic molecules like Polycyclic Aromatic Hydrocarbons (PAHs) that give fruits and vegetables their orange-red color, see Cuzzi et al. [2009] for a discussion.

Broadly speaking, the optically thinner C-ring and Cassini division are more polluted by some spectrally neutral non-icy material than the A-ring or B-ring, making them darker at visual wavelengths and decreasing the strengths of the near-IR water ice bands; this is the natural outcome if the darkening material is deposited from extrinsic meteoroid bombardment [Cuzzi and Estrada 1998; Elliott and Esposito 2011], see also Cuzzi et al. 2009 for a review. More recent results from CIRS thermal models give the ring particle bolometric albedo; another measurement of their non-icy pollutants. It is interesting that, like inferences from visual wavelength reflectivities, the bolometric albedos are not only lower in the C-ring and Cassini division, but also vary smoothly across the sharp A-ring and B-ring boundaries [Morishima et al. 2010], as generally predicted by ballistic transport models.

Cassini's late-orbit in situ observations find plenty of organic material and some silicates, but no discernible free metal or metal oxides … .

Cassini's late-orbit in situ observations find plenty of organic material and some silicates, but no discernible free metal or metal oxides—see section entitled Composition of Rings from Ring Ejecta for details. Moreover, the most recent Cassini and non-Cassini studies using both classical and Monte-Carlo ring radiative transfer models agree that the spectra are more consistent with reddish organics than with other suggested materials [Ciarniello et al. 2019; Cuzzi et al. 2018b]. However, even the best current regolith scattering models simplify the physics and involve several parameters. Because different flavors of Hapke-like regolith scattering models lead to systematic, model-based uncertainties in absolute abundances at the factor-or-several level, or even worse, quantitative inferences about abundances must be treated with caution. For instance, Hedman et al. [2013a] interpreted fine-scale radial color variations in terms of regolith grain size, but this may have been because of the limitations of their (classical) model, whereas other secondary optical-depth-related effects may likely be the cause. On the other hand, Cassini's UV spectrometer UVIS observed the strong 170 nm water ice absorption edge and how it varies across the rings [Bradley et al. 2010, 2013]. These analyses provide a sensitive measurement of the regolith grain size, which can remove ambiguities in regolith models at comparable wavelengths and lead to absolute abundances of non-icy material—see section entitled Ring Particle Composition and Size for more discussion of grain size effects. Therefore, while the compositional debate has clarified regarding overall composition, there is a need for considerably more work regarding radial variation and inference of quantitative abundances of non-icy material, see section entitled Non-Saturn-System Science Results.

Other new contributors to the ring composition were the CIRS far-IR capability[2] and the Cassini 2.2 cm Titan Radar Mapper (RADAR), used in radiometer mode[3]. These observations have considerable historical motivation, as microwave observations were the first to constrain the ring composition as nearly pure water ice particles of cm-m size, see Esposito et al. [1984] for a review. The basic observation is that the brightness temperature of the rings drops from the physical temperature in the thermal IR, to a small fraction of it in the microwave (thus requiring a low particle emissivity). CIRS was able to get ring spectra covering the transition spectral range between thermal IR and several hundred micron wavelength, resolving inconsistent Voyager-era observations [Spilker et al. 2005, 2018]. CIRS and 2.2 cm radiometry was used to create sensitive high-resolution maps of the very low microwave brightness temperature [Zhang et al. 2017a, 2017b]. Microwave radiometry is unique because the long wavelengths penetrate to depths of several meters in cold water ice that has a very low microwave absorption coefficient, thus microwaves sample the bulk composition of the ring particles in a way that micron and submicron wavelengths cannot. The Cassini 2.2 cm radiometry had sufficiently high resolution to separate the A-ring, B-ring, and C-ring into dozens of radial bins and greatly improved on groundbased interferometry by setting upper limits of a fraction of a percent on non-icy material in the A-ring and B-ring.

Analysis of the 2.2 cm radar radiometry observations also found that the C-ring (with up to 6% non-icy material uniformly mixed) is much dirtier than the A-ring and B-ring [Zhang et al. 2017a, 2017b]. The assumption of uniform mixing may seriously underestimate the C-ring non-icy material abundance. Constraints on surface mass density from a handful of spiral density and bending waves strongly suggest that the particles in the same belt of the central C-ring, where unusually high abundances of silicates are found, have an internal density several times higher than water ice; far heavier than explained by a mere 6% in uniformly mixed silicate dust. The situation suggests buried solid chunks of non-icy material (silicate or carbonaceous) in large volume fraction. This rubble belt is what we might expect the remains of a disrupted core of a differentiated object to look like. However, modeling the microwave emission/scattering problem in the main rings is very difficult since the particle sizes and separations are not much larger than the wavelength and are in the near field of each other. Therefore, approximations are needed even in the very best current models, leading to some degree of compositional uncertainty. Moreover, these analyses are insensitive to the nature of the non-icy material.

Recent comparisons of spectral properties of the main rings with those of the ringmoons and classical icy moons are provided by Filacchione et al. [2012, 2013, 2014], and other recent reviews are by Cuzzi et al. [2009, 2018a]. For complementary discussion of the ring composition based on in situ observations (not part of the AO objectives), which are especially relevant to the D-ring, see section entitled Ring Age and Origin. The so-called diffuse rings (D-ring, E-ring, F-ring, and G-ring)

[2] It had been hoped that the longest wavelength channel of CIRS – advertised as 0.5mm wavelength, but more realistically 1 mm, could be used as a radiometer in this way. However, complicated calibration problems with the Michelson interferometry technique precluded this even after considerable effort by the team.

[3] Little was proposed or expected along the lines of ring science from RADAR in the AO or early discussions, as the team was exclusively focused on Titan. However, as the mission went on and the antenna beam was carefully calibrated, the very low ring brightness temperature was mapped even in the presence of the 10-times-brighter, huge globe of Saturn looming in the complex sidelobes.

and smaller rubble belts are discussed in the section entitled Dust and Meteoroid Distribution, both regarding structure and composition.

SIZE DISTRIBUTION

Even before Voyager, it was known from groundbased microwave observations that by far most of the main ring particles were in the cm-few meters size range [Orton et al. 2009], and for this reason microwave wavelengths were expected to be the most powerful at specifying their details. To this end, Cassini's observation planning incorporated 135 radio occultations of the main and F-rings, at three wavelengths: 0.94, 3.6, and 13 cm. These occultations provide the direct-path optical depth at all three wavelengths, clearly showing local and regional differences in the abundance of the smaller particles (a few cm in radius). In addition, the off-axis scattering (so-called bistatic scattering) of the radio beam can be used to constrain variations in the particles at the large-size end of a (usually) powerlaw size distribution, as well as the slope of the powerlaw, for example, Zebker et al. [1985]; Cuzzi et al. [2009]. The RSS occultation profiling observations have been reduced, corrected for diffraction, and provided to the Rings Node of the PDS, some examples are shown in Cuzzi et al. [2009] Figures 16.1a–16.2. Distinctions as subtle as changes in the slope of the powerlaw size distribution and the minimum and maximum particle size between typically a few mm and a few meters can be discerned. In addition, stellar occultations contribute information on the relative abundance of smaller particles.

Some generalities can be extracted even at this preliminary stage of the investigation. The fraction of small particles increases outwards through the A-ring based on the RSS data, consistent with more vigorous collisions associated with the increasing radial density of resonances and spiral density waves [Cuzzi et al. 2009; Becker et al. 2016; Jerousek et al. 2016].

In the RSS data, C-ring "plateau" structures show local drops in the differential optical depth, characteristic of locally fewer (short-)wavelength-size particles, and a similar effect is seen crossing from the outer C-ring to the inner B-ring, and from the outer Cassini Division to the inner A-ring; with the optically thicker rings having relatively fewer wavelength-size particles lying near the small end of the size distribution [Cuzzi et al. 2009].

Stellar occultation variance data[4] from UVIS provides an independent and complementary particle size determination to the RSS data. Analysis of this type reveals that all of the C-ring plateaus and narrower embedded ringlets have a smaller mean particle size compared to the background C-ring. The background C-ring has an undulating optical depth over scales of hundreds of km, and effective particle size correlates positively with this structure, this may suggest size-dependent dynamical transport within the ring. The innermost 700 km of the B-ring, and regions around the strong resonances in the A-ring, exhibit different effective particle sizes based on occultation variance (even though self-gravity wakes in these regions dominate the signal). There is a marked decrease in effective particle size coinciding with the Mimas 5:3 bending wave in the

[4] Showalter and Nicholson [1990] introduced this technique to relate the excess variance in the occultation signal (about a radially variable, locally defined mean) to the size of the largest local particles.

outer A-ring. This and other observations suggest a vertically extended haze of small particles across the wave; oddly, the effect is not seen in the nearby density waves where collisions might be expected to be even more vigorous. The variance in the Cassini Division ramp reveals the particle size distribution there to be more similar to the A-ring than to the Cassini Division, with a discrete increase in effective particle size at the inner edge of the ramp. On the other hand, the comparable C-ring–B-ring boundary transition is more gradual in variance and implied particle size [Colwell et al. 2018].

Because the optical depth does change abruptly by a factor of several, there must be a corresponding abrupt change in the opacity at these locations, requiring a change in the particle size distribution.

More information on particle sizes can be gained by comparing the local surface mass density from wavelengths of spiral density and bending waves, see Colwell et al. [2009]; Schmidt et al. [2009], with the local optical depth. For identical particles, the opacity (ratio of optical depth to surface mass density) is inversely proportional to particle size. Based on a number of observations of spiral density waves, there seem to be only very smooth, or no, dramatic changes in surface mass density across the plateaus or across the inner A-ring boundary [Tiscareno et al. 2013a; Colwell et al. 2009], see also the section entitled Gravitational processes. Because the optical depth does change abruptly by a factor of several, there must be a corresponding abrupt change in the opacity at these locations requiring a change in the particle size distribution. The sense of this is that the particles are on average smaller in the plateaus, and in the inner A-ring and B-ring, than in adjacent material, consistent with the variance data noted above. However, RSS occultations show that these same regions have fewer cm-size particles, requiring either that there must also be fewer large particles or that the largest particles are smaller, in the plateaus and similar regions. All together this suggests narrower size distributions for the plateaus, and inner A-ring and B-ring, than for their surroundings; relatively fewer particles at both size extremes. There is currently no explanation for this strong structural control on particle size, with very abrupt boundaries.

An important kind of size distribution is the size distribution of regolith grains on the surfaces of ring particles. While not what a dynamicist would call a ring particle, these grains along with their underlying material composition determine the spectral signature at any wavelength. Regolith grain sizes are usually best determined in and around strong absorption bands. UVIS, for instance, sees the strong water ice edge at 170 nm, and from the details of its position determines a regolith grain size of about 5 microns [Bradley et al. 2010, 2013]. However, at longer wavelengths (the near-IR water bands) larger grain sizes in the tens of microns are generally derived [Cuzzi et al. 2009; Clark et al. 2012; Filacchione et al. 2012, 2013]. This is consistent with the idea that shorter wavelengths sense and are scattered by smaller scale structures. Indeed, even before Cassini, models by Poulet and Cuzzi [2002] and Poulet et al. [2003] of Earth-based spectra of the rings covering the 0.3–4.5 um spectral range required very broad regolith size distributions; from 10 microns to several millimeters. Analyses of the long-wavelength roll off from much longer wavelength CIRS data [Spilker et al. 2005], and a 30 micron ice absorption feature [Morishima et al. 2012] suggest (not

surprisingly) a broad size distribution from tens of microns to centimeters radius with the larger ones perhaps starting to merge from regolith particles to freely-floating particles. Much more work is needed with improved regolith radiative transfer models and broader spectral ranges.

The so-called diffuse rings (D-ring, E-ring, F-ring and G-ring) have their own distinct size distribution; generally dominated by micron-sized particles that diffract, rather than backscatter, light at UV, visual, and NIR wavelengths (see section entitled Dust and Meteoroid Distribution).

Ring-satellite interaction (R_AO3)

Investigate interrelation of rings and satellites, including embedded satellites.

The first actual sighting of a small moon embedded in a clear gap was Pan, in the A-ring Encke gap … .

The first actual sighting of a small moon embedded in a clear gap was Pan, in the A-ring Encke gap [Showalter 1991], see also Colwell et al. [2009]; Orton et al. [2009]. Cassini quickly found a second example: Daphnis, in the Keeler gap, has an inclined orbit and the wavy edges it imparts to the gap flap vertically [Weiss et al. 2009]. The known dimensions and masses of these objects [Porco et al. 2005, 2007], combined with the estimated ring viscosity, provides our best validation of the shepherding torque theory [Goldreich and Tremaine 1980, 1982; Schmidt et al. 2009]. Cassini then embarked on an extensive systematic mapping of the other multiple empty gaps in the Cassini Division and C-ring over the duration of the mission, coming up empty handed, and (even though not every longitude of every gap was mapped) concluding that these gaps do not seem to be cleared by moonlets [Spitale 2017], at least based on the shepherding torque theory as currently understood [Schmidt et al. 2009]. Clues about other gap-clearing processes may be found in some of the details of the edge locations of the Cassini Division gaps [Nicholson and Hedman 2010; Spitale and Porco 2010; French et al. 2016a]. However, there are no corresponding clues regarding the few C-ring gaps lacking moonlets, which may instead be explained in the context of whatever mystery process generates the C-ring plateau ensemble, with which the unexplained gaps are associated. It is ironic that the Voyager imaging team redirected resources late in the planning phase to test a (then-new) hypothesis for gap-clearing by searching for gap-embedded moonlets, but resource and time constraints forced a choice of targeting only one gap, and as it turns out, the Cassini Division where they looked was not the right place [Smith et al. 1982].

Ring edges can also be maintained by single, isolated resonances, as at the outer edges of the B-ring (Mimas 2:1 resonance) [Spitale and Porco 2010, and references therein] and the A-ring outer edge (Janus 7:6 resonance) [Porco et al. 1984]. Recently El Moutamid et al. [2016c] and Tajeddine et al. [2017a] showed in detail how Janus actually is able to create an abrupt edge for the outer A-ring and restrain its spreading, even as it swaps orbits back and forth with Epimetheus, in somewhat of a team effort with all the other ringmoons and resonances acting on different parts of the A-ring, so the classical shepherding theory seems to be in good shape. The kinky, stranded

F-ring has a more complicated, often chaotic, relationship with its nearby moons, though (see section entitled F-ring).

A special kind of embedded moonlet is one that is too small (smaller than 1 km radius) to actually open a gap; these were predicted by Spahn et al. [1994], but most Cassini scientists were surprised to actually see some, initially in the Saturn Orbit Insertion (SOI) images [Tiscareno et al. 2006]. These have been dubbed “propellers” by virtue of the disturbances they create, which are too weak to prevent viscosity from backfilling the disturbance before the next encounter of the moonlet with the same material. It seems there are on the order of a million of these objects in the A-ring, and they are confined mostly to three distinct bands in the A-ring [Sremčević et al. 2007; Tiscareno et al. 2008]. There have been reports of propellers in the B-ring as well [Sremčević et al. 2012, 2013, 2014a, 2014b]. It is not currently understood whether these objects are shards of a ring parent, or are somehow spontaneously forming and perhaps dispersing in place [Esposito et al. 2012]. The three A-ring propeller bands are anti-correlated with the halos of large spiral density waves, and correlated with the strength of self-gravity wakes, which might favor the local formation idea or might simply indicate changes in the photometric balance or local viscosity that causes propellers to be visible. A subset of much larger objects, dubbed Giant Propellers, was discovered, which could be tracked and found to be evolving in semi-major axis [Tiscareno et al. 2010]. This discovery motivated significant dedicated observing during the extended mission (see section entitled New Ring Structure). Meanwhile, the theory of these disturbances has been actively discussed and continues to advance [Schmidt et al. 2009; Crida et al. 2010; Pan and Chiang 2010, 2012; Rein and Papaloizou 2010; Pan et al. 2012; Bromley and Kenyon 2013; Tiscareno 2013; Seiler et al. 2017; Seiß et al. 2018].

A possible physical extension of these objects to smaller sizes has been seen in the optically thicker bands of the C-ring (including the plateaus) and Cassini Division (including its outer ramp); so-called ghosts or partial clearings appear in UVIS occultations with very small lengthscales [Baillié et al. 2013]. These are thought to be caused by relatively large ring particles (maybe meters to tens of meters in size) smaller than the A-ring and B-ring propellers (objects so small would not clear gaps in the generally higher optical depth, and more strongly stirred, A-ring and B-ring). These objects would need to be more than three times larger than the largest ring particle in a powerlaw size distribution in order to create the ghost clearings.

Fleeting glimpses of what appear to be embedded Keplerian objects have also been obtained near the edges of several rings and ringlets. At the outer edge of the A-ring, the so-called “Peggy” object was seen briefly [Murray et al. 2014], seemingly getting ready to break free of the main rings. This exciting moment might, it was thought, allow the object to be spun away from the rings due to ring torques such as modeled by Charnoz et al. [2010]; an effect by which the age of the rings might be constrained (see section entitled Ring Origin and Age). However, Peggy actually was reabsorbed back into the rings and apparently broke into several pieces, proving that leaving home can be difficult. Moderately large Keplerian objects, but still too small to be seen directly, were also seen near the edges of the A-ring Keeler gap [Tajeddine et al. 2017b], in the Huygens ringlet of the Cassini Division [Spitale and Hahn 2016], and near the outer edge of the B-ring itself [Spitale and Porco 2010—see also Cuzzi et al. [2018a]. It has been suggested that many or even all of these

objects are transient, forming by compaction due to satellite perturbations, and then being disrupted as they increasingly stir the regions around them [Esposito et al. 2012].

Finally, it cannot be forgotten that all the wonderful dynamical relationships we are starting to understand between the rings and various moons depend on a good understanding of the orbital dynamics of the moons themselves, and the so-called ringmoons in particular, that interact strongly with the rings [Spitale et al. 2006; Jacobson et al. 2008; Tajeddine et al. 2013]. Additional results can be found in the ISS Instrument Science Results. Of special importance is the paradigm-breaking observational result of Lainey et al. [2017] that the midsize icy moons of Saturn, from Mimas through at least Rhea, are tidally evolving outwards much faster than had been previously assumed based on traditional tidal "Q" theory. This was extremely surprising, because Saturn's interior had been thought to be quite non-dissipative, like Jupiter, with a high "Q" value (see section entitled Saturn System Science Results). A more recent tidal theory suggests that "Q" is highly frequency dependent, and that moons get trapped on a comb of low-Q frequencies that slowly decrease as Saturn's interior structure evolves, driving the entire set of moderate-sized icy moons outward at a more or less distance-independent rate instead of the strongly distance-dependent rate of traditional tidal theory—see for example, Fuller et al. [2016]. This new perspective has profound implications for the origin and (now increasingly believed to be) geologically youthful age of the rings (see section entitled Ring Origin and Age).

Dust and meteoroid distribution (R_AO4)

Determines dust and meteoroid distribution both in the vicinity of the rings and in interplanetary space.

THE DIFFUSE RINGS

The so-called diffuse rings (D-ring, E-ring, F-ring and G-ring) are best studied by tracing their micron-size particles. Such small particles scatter UV, visual, and near-IR light into small solid angles in the forward direction so they may be more easily detected than in the lower brightness of their larger particles, which is spread over more angles near backscattering and also may be subject to the low brightness of individual particles. In all these cases where only fine dust belts are observed, it is generally accepted that a larger-particle skeleton (or some small parent moonlet) must be present to resupply the micron-sized material, which is rather quickly lost [Burns et al. 1984; Hedman et al. 2018a]. Based partly on observations of charged particle depletions [Van Allen 1982]—see also Section 3.1 Discipline Science Results chapter entitled MAPS for Cassini-based examples; the G-ring has long been known to contain an underlying rubble belt or arc of macroscopic particles—see reviews by Orton et al. [2009] and Hedman et al. [2018a]. Cassini discovered that the ultimate source of this rubble belt is a 0.5 km size, highly non-spherical object called Aegaeon, which has a very dark primitive-body type surface [Hedman et al. 2011a]. Moreover, Aegaeon is trapped in a 7:6 resonance with Mimas [Hedman et al. 2007c, 2010].

Several other dusty arcs of material were discovered, supplied by the small moonlets Anthe, Pallene, and Methone—of these, Methone and Anthe are trapped in Mimas resonances [Hedman et al. 2009b]. A composite dusty ring phase function and size distribution was obtained from wide phase angle coverage of the D-ring and G-ring, for application to so-called Debris Disks around young stars [Hedman and Stark 2015]; a certain similarity in the two ring phase functions may point to some family and/or process similarity in the particles; such as an aggregate, fractal structure. The D-ring shows several kinds of time variability, and is discussed more in the section entitled Ring Temporal Variability. Also, the giant, diffuse Phoebe ring, discovered in 1999 by the Spitzer Space Telescope [Verbiscer et al. 2009], was further constrained in extent, dynamics, and particle size using shadow-edge imaging observations [Tamayo et al. 2014, 2016].

A disadvantage of necessary reliance on forward scattering for the diffuse rings, is that it is essentially diffraction, and only weakly dependent on composition, so the composition of these rings is not quite as well known. Even when there is some signal in backscattered intensity or reflectivity, it remains problematic to derive even albedos for the large F-ring and G-ring particles (whose scattering would be compositionally diagnostic) because their optical depths are variable and/or small, and so uncertain. The F-ring is known to be dominated by crystalline water ice [Vahidinia et al. 2011; Hedman et al. 2011b], but may be significantly polluted by drifting G-ring material [Clark et al. 2012]—see also Cuzzi et al. [2018a], Figure 3.22, and the section entitled F-ring for more discussion. By comparison, the composition of the E-ring is known very well from CDA in situ sampling (mostly water ice, with embedded organics and salt, all characteristic of the underground Enceladus Ocean from which it comes), and its structure is discussed in the section entitled Changing Rings. In situ sampling of nanoparticles in the D-ring is discussed in sections entitled Ring Magnetosphere and Determination of Ring Mass.

THE EXTRINSIC (INTERPLANETARY) MASS FLUX - A PRIMARY GOAL OF CASSINI

The CDA instrument [Srama et al. 2005] estimated detecting 100 extrinsic particles of micron-size and larger. However, early in the mission it started to look difficult or impossible to measure it directly (it is a very dusty system in reality), so an indirect approach was explored to look for dust ejecta haloes around Rhea and Tethys, by analogy to Galileo results at Jupiter [Sremčević et al. 2005]. This led to only upper limits and an initial conclusion that the extrinsic meteoroid flux was lower than previously assumed. However, the basic direct approach simply counting up the detections and velocities of small particles with identifiably extrinsic orbits was ultimately successful partly due to the much longer time baseline of the CSM (13 years) relative to the baseline mission. The lack of indirect detection (satellite dust haloes) was reconciled after the fact by uncertainties in the ejecta yield model. For example, the ongoing snowfall caused by Enceladus' geysers might have influenced/changed the mechanical surface properties of Rhea and Tethys compared to the Jovian icy moons. Future analyses of thermal inertias might provide useful constraints on satellite surface properties, in this regard.

The CDA meteoroid mass flux measurement works as follows [Kempf et al. 2019], see Section 3.2 Instruments Science Results chapter entitled CDA. For each particle detected entering

the instrument there is an instrumental ambiguity that allows two equally valid predetection velocity vectors. A lower limit to the incident mass flux comes from only the 25 particles for which both velocity vectors trace back to extrinsic projectiles, from beyond Saturn. An upper limit of a sort also includes the 75 or so particles for which only one of the velocity vectors requires an extrinsic origin. Because the size distribution of the detected particles is not well known, the largest particles might carry most of the mass, and their rarity suggests that the nominal detection values could be a lower limit. For instance, a solitary 250 μm particle was not included in the mass flux calculations (including it would increase the mass flux by a factor of five) and another year of mission time might have captured more large particles. Future, more detailed (perhaps Bayesian) analyses might refine the uncertainties more, but at present it seems that the nominal CDA minimum flux is conservative. The values for the minimum flux at infinity (before gravitational focusing by Saturn) are within a factor of order unity of pre-Cassini assumptions [Cuzzi and Estrada 1998]. However, the CDA discovery that the pre-Saturn orbits were dynamically Kuiper Belt object (KBO)-like (low eccentricity and inclination) rather than comet-like (and thus have lower encounter velocities), leads to an order of magnitude increase in Saturn's gravitational focusing factor and thus in the flux at the rings. The implications of this new result for models of ring structural and compositional evolution, which have multiple parameters [Estrada et al. 2015] are not yet well understood, but they are unlikely to allow a ring age older than previous estimates of some hundreds of millions of years.

Perhaps a simple, large field-of-view (FOV), NIR photometer experiment to monitor impacts might be considered for a future mission.

Along the lines of mass flux into the rings, we should mention flux at larger sizes as perhaps providing additional constraints on ring evolution; as yet, no effort has gone into merging these datasets and results. An observation by RPWS only reported at meetings [Gurnett et al. 2004] may suggest impacts by dozens of particles during the 30 minutes Cassini was skimming across the face of the rings at SOI. Significant theoretical development is needed to translate these observations into responsible projectile sizes (sand-grains?), but if this can be done, the rates would surely be of interest. Impact ejecta trails from a handful of meter-sized particle impacts were imaged by ISS [Tiscareno et al. 2013; Schmidt and Tiscareno 2013]. UVIS mounted an early attempt to detect actual impact flashes themselves, but subsequent thought and modeling concluded that the flash could only be seen in the near-IR [Chambers et al. 2008] so the UVIS searches were discontinued. Perhaps a simple, large field-of-view (FOV), NIR photometer experiment to monitor impacts might be considered for a future mission. Finally, as discussed in the section entitled Ring Temporal Variability, there is evidence for multiple impacts on the rings by 1–10 km size objects over decades and centuries.

Ring magnetosphere-ionosphere interactions (R_AO5)

Studies interactions between the rings and Saturn's magnetosphere, ionosphere, and atmosphere.

It has long been known that the rings have an atmosphere of their own due to photosputtering and meteoroid bombardment, and interact with both the magnetosphere and the planet, even reducing the ionospheric electron density [Shimizu 1982; Connerney and Waite 1984]. During SOI, Cassini obtained the first-ever in situ measurement of the ring atmosphere, and it was a big surprise. It had been expected to be dominated by water products (WP) (molecules and ions of H_2O and its fragments), but instead Cassini Plasma Spectrometer (CAPS) found it was dominated by neutral and ionized O and O_2 [Tseng et al. 2010]. The observations and theory are reviewed in Cuzzi et al. [2009]; essentially, WP recombine on ring particle surfaces, but O and O_2 do not, building up in the ring atmosphere without freezing out or adsorbing onto ring particle surfaces, and ultimately filtering out to the magnetosphere and into the planet [Tseng et al. 2010]. Since that review, the effect has been modeled in more detail, and the observed seasonal variation of magnetospheric oxygen ions transported from the rings (see Section 3.1 Disciplines Science Results chapter entitled MAPS) suggests that photosputtering of ring ices dominates over material from Enceladus in producing the ring atmosphere [Tseng et al. 2010, 2013; Elrod et al. 2014]. This discovery of the ring atmosphere alone would satisfy the AO objective, but indeed during the RG and GF orbits, Cassini discovered far more about the particulate component of the ring atmosphere and its flux into the planet; the so-called ring rain long speculated upon, for example, Connerney and Waite [1984]. We discuss this in detail in the section entitled Ring Age and Origin.

The D-ring is now known to be embedded in a high-energy-particle radiation belt that is separated from Saturn's main radiation belts [Kollmann et al. 2019; Roussos et al. 2019]. This may help explain its possible shortage of water ice (see section entitled Composition of Rings from Ring Ejecta). The diffuse E-ring and G-ring interact in more intimate ways with the magnetosphere; their tiny grains get charged and undergo electromagnetic forces (see section entitled Electromagnetic and Radiative Processes).

Extended Mission (CSM) Objectives

The objectives below were developed in 2010, to prioritize upcoming planning by focusing on specific problems, either unresolved AO goals or unexpected new phenomena, and to take advantage of the unique geometries of the CSM.

Changing rings (RC1a)

Determines the seasonal variation of key ring properties and the microscale properties of ring structure, by observing at the seasonally maximum opening angle of the rings near Solstice.

The emphasis here is on observing at the seasonally maximum opening angle of the rings near Solstice. The dominant operative intention was to take advantage of the maximum ring opening angle as seen from Earth and the Sun to: a) allow CIRS to determine the energetics of thermal heating and cooling of the rings as they opened to their maximum opening angle to the sun; and b) allow RSS occultations to penetrate the most opaque parts of the rings (the central B-ring), which they had not yet been able to do even during the maximum opening angle allowed

during Prime Mission (21°). The difference relative to true maximum opening angle of 23.7° can be critical for RSS, as it appears in the exponential of the optical depth term. The objective was very well satisfied, in that 36 more radio occultations were obtained, with various combinations of resolution and sensitivity, at opening angles larger than available during prime mission and more suitable for probing the dense B-ring. The data have been reduced and deposited in the Rings PDS node at 1 and 10 km spatial resolution. CIRS also obtained data over a wide range of opening angles; one important conclusion has to do with the seasonal cooling of the rings through equinox; their minimum temperature is considerably larger than instantaneous thermal equilibrium with Saturn's reflected and emitted energy, constraining the internal density of the particles (at least in the A-ring where the model was applied) to be closer to solid ice in the central A-ring than in its inner or outer regions [Morishima et al. 2016]. Perhaps this can be correlated with the radial variation of self-gravity wakes and/or the radial distribution of propeller objects.

When this goal was written, it was still not known as to whether the spokes would vanish again, and if so, exactly when and under what geometrical conditions. Indeed that situation is now well understood in terms of photocharging of the main rings (see section entitled Electromagnetic and Radiative Processes).

The diffuse E-ring, composed largely of micron-sized grains jetted out of Enceladus, deforms and changes shape with the seasons in response to the elevation angle of the sun, as solar radiation pressure influences the orbits of these tiny grains [Hedman et al. 2012].

The waxing and waning of the magnetospheric oxygen ion content is dominantly seasonal; implicating photosputtering of ice in the main rings rather than impacts by grains from Enceladus, one previous candidate [Tseng et al. 2013].

Ring temporal variability (RC1b)

Determines the temporal variability of ring structure on all timescales up to decadal for regions including Encke gap, D-ring, F-ring, and ring edges by substantially increasing the cadence and time baseline of observations.

The rings are changing before our eyes. The F-ring may be the most extreme example of time variability, and merited its own strategic objective (see section entitled F-ring). Here we discuss other aspects of ring temporal variability.

The sharp edges of the A-ring and B-ring flop around loosely, revealing the fluid nature of the rings. The A-ring outer edge seven-lobed structure derives from a 7:6 resonance with (mostly) Janus, and it reorganizes itself, diminishing in amplitude, when Janus swaps to its outer orbit and the resonance moves off of the A-ring edge [Spitale and Porco 2009; El Moutamid et al. 2016c]. The B-ring outer edge is more complicated, showing the predicted two-lobed forcing of the Mimas 2:1 resonance, but in addition, showing interference with m = 1, 2, and 3 patterns that are probably free modes driven by ring pressure and viscosity. Sometimes the pattern almost vanishes because

of this interference [French et al. 2010; Hedman et al. 2010b; Esposito et al. 2012; Nicholson et al. 2014; Spitale and Porco 2010]—see section entitled Viscous Processes.

Saturn's innermost ring (D-ring) is only visible with effort and in favorable geometry. However, after the F-ring fireworks, it has provided some of the most interesting evidence for time variations (usually observed by virtue of its fine dust component, in forward scattering geometries, as discussed in the section entitled The Diffuse Rings). Hedman et al. [2007b] first noticed that its structure of irregularly spaced bands or belts had changed dramatically since Voyager. They also pointed out a pattern that they interpreted as a vertical spiral ripple, and suggested that the ripple was the result of an ongoing wrapping up by differential node regression of a tilted mean ring plane. From the wavelength of the wrap, which shortens with time, they dated the event to the early 1980s. Hedman et al. [2011c] found the ripple to extend through the C-ring, and suggested that the tilt was imposed by an impacting stream of rubble, perhaps from a disrupted, 1–10 km size, Shoemaker-Levy-9 type object, with an extended node crossing the D-ring and C-ring. Hedman et al. [2015] determined, from further analysis, that the event may have had two parts, separated by months. Hedman and Showalter [2016] subsequently found pattern evidence for two other disturbances that occurred in 1979 (in Voyager data) and 2011. Marouf et al. [2011] discovered a similar pattern in the C-ring, from higher-resolution radio occultation data, that they interpreted as two events, separated by 50 years that occurred in the late 1300s. It is fascinating that the rings still bear silent witness to these long-lasting scars of cometary impacts. A related example of time variability is ongoing impacts onto the ring by discrete particles large enough to create detectable disturbances; the little cousins of these ripple-forming comet-size objects. Impacts by meter-size particles have been observed directly; once a leading candidate for triggering spokes (see section entitled Electromagnetic and Radiative Processes), the connection between the observed meter-size impact rates and spoke formation rates has not been pursued in depth. These impact effects were discussed in the section entitled The Extrinsic (Interplanetary) Mass Flux.

The D-ring and C-ring show two other, still unexplained, kinds of time variation. Hedman et al. [2014b] found that one of the most prominent bright ringlets in the D-ring, also seen by Voyager, is moving inwards at more than 2 km/year, and apparently moved outwards to its current position between Voyager and Cassini. The ringlet also has strong azimuthal clumpiness that seems stable, but cannot be associated with any plausible resonance with either some known moon, or some known planetary interior modes or rotating structures; all in all it is a puzzling dynamical feature. Also, there are time-variable aspects to several C-ring spiral density waves that appear to be driven by density fluctuations fixed to Saturn's internal structure and rotating with its winds; so-called tesseral resonances (see section entitled Gravitational Processes). Hedman et al. 2017, 2018b; Hedman and Nicholson 2014] have found that some of these wavetrains seem to be drifting inwards at about 1 km/year, as if the density fluctuations causing them were moving in latitude or depth inside the planet. The D-ring also revealed a new set of bright clumps near the end of the mission, possibly related to time variation in the INMS GF observations (see section on Composition of Rings from Ring Ejecta).

F-ring (RC2a)

Focuses on F-ring structure, and distribution of associated moonlets or clumps, as sparse observations show clumps, arcs, and possibly transient objects appearing and disappearing.

Because of the strong time variations seen during prime mission, the F-ring became a central focus for Cassini imaging observations during CSM. The F-ring lies about 3000 km outside the A-ring edge, and is unique in the family of planetary rings. Faintly glimpsed by Pioneer 11, its kinky, multi-stranded structure was revealed in Voyager images to be dominated by small dust grains, and Voyager radio and stellar occultations showed it to have a very narrow core of larger objects. Earth-based observations between Voyager and Cassini showed it to be highly variable, with large clumps coming and going, having orbital periods that differed slightly from that of its central strand [McGhee et al. 2001]. As it was straddled by the 100 km diameter ringmoons Prometheus and Pandora, classical shepherding theory was quickly proposed to explain its survival. However, almost immediately, problems arose with that interpretation, growing over the years when it was realized that not only were the so-called shepherds on chaotic orbits themselves, but objects orbiting between them were excited to even more chaotic orbits [Cuzzi et al. 2014]. In fact, Cassini very quickly observed some of these objects (2004S6, etc.) [Porco et al. 2005] on orbits that crossed the F-ring, but could not be tracked for more than a few months before they vanished [Cooper et al. 2017]. Meanwhile, large jets of material were seen splashed out from the central core due to collisions by these careening objects [Charnoz et al. 2005; Murray et al. 2008; Becker et al. 2018], and evidence was found for smaller, unseen objects embedded within the F-ring strands themselves. Dynamical models showed how the perturbations of Prometheus alone could explain the alternating streamer-channel appearance of the F-ring [Murray et al. 2005; Beurle et al. 2010].

Several new classes of embedded objects were inferred and modeled, based on often faint and initially obscure patterns seen to come and go. Mini-jets (small spikes poking out of the central strand) were catalogued and understood as caused by large embedded objects (meters or tens of meters in size perhaps) colliding at low (few m/sec) speeds within the dense central ring strand [Charnoz 2009; Murray et al. 2008; Esposito et al. 2008; Beurle et al. 2010; Albers et al. 2012; Meinke et al. 2012; Attree et al. 2012, 2014]. Fans or localized regular brightness fluctuations were shown to be due to small embedded objects on slightly eccentric orbits relative to the F-ring [Murray et al. 2008]. Some of these fans were localized to parts of the ring where Prometheus compressed ring material, perhaps actually forming new small moonlets [Beurle et al. 2010].

RSS occultations only detected the F-ring's very narrow (< 1 km) true core of cm-and-larger-size particles about 1/3 of the time, showing it had to be azimuthally broken and discontinuous. Using these observations, a new theory was developed in which the stability of the true core, in the presence of strong orbital chaos driven locally by Prometheus, seems to be due to longitudinal confinement into separated clumps or arcs by a corotational resonance in which the stable clumps never encounter Prometheus at its apoapse where strong chaos-inducing perturbations can result [Cuzzi et al. 2018c], see also Albers et al. [2012]; Cooper et al. [2013]. The reason why only this one of many nearby corotational resonances is occupied remains unclear. This arrangement of incomplete arcs of macroscopic particles must occasionally make small

adjustments, given the occasional chaotic changes in Prometheus' orbit to which the clumps must readjust. Hedman et al. [2011b] observed variations in crystalline ice band depth due to variations in the relative abundance of macroscopic bodies and dust, which have yet to be correlated with the RSS clumping. Large objects forming in fans, and usually outside the very narrowly defined stable true core orbit [Cuzzi et al. 2014, 2018c], can become strongly perturbed by Prometheus and evolve into 2004S6-like objects, ultimately recolliding with the F-ring at high speeds. Indeed, while 2004S6 was tracked in 2006–2008 as it collided with the F-ring several times and then lost, similar objects have since appeared. Different frequencies and intensities of such big eruptions as seen by Cassini and by Voyager observations underline the sporadic nature of these variations [French et al. 2012, 2014].

Ring age and origin (RN1a)

Constrains the origin and age of the rings by: a) direct determination of the ring mass; and b) of the composition of ring ejecta trapped on field lines.

Over the years the ring composition has emerged as perhaps the best gauge of ring age and clue to ring origin. While ring composition is powerfully addressed using traditional remote sensing techniques (see section entitled Ring Particle Composition and Size), this objective focused on in situ measurements that were only achievable during Cassini's RG and GF orbits.

Determination of ring mass

It was not known, when Cassini was initially planned, that we would be able to obtain a direct measurement of the ring mass; this only became possible in the CSM GF orbits when the spacecraft was able to fly between the rings and the planet 22 times. The original AO mission plan was to constrain the ring mass by measuring the ring optical depth and particle size distributions together, and sample all available spiral density waves, using stellar and radio occultations. However, because of the possible ambiguities associated with hidden mass in the B-ring that arose during the prime mission (see section entitled Gravitational Processes), six complete close passes were allocated in the GF orbits, during which the spacecraft remained quiet while RSS transmitted a carrier signal to Earth, to allow the small gravitational effects of the rings to be separated from those of Saturn; a mini-Juno mission. The details of the technique, and difficulties encountered, are described by Iess et al. [2019] and in this volume. Unexpected and probably azimuthally variable internal properties of the planet (very unlike those of Jupiter) contaminate the gravitational signature of the rings, increasing the measurement uncertainty to perhaps 50% of the signal. It is puzzling that, if the RSS variance is interpreted as internal mass irregularities, the amplitude of these seems considerably larger than would be

It was not known, …, that we would be able to obtain a direct measurement of the ring mass; this only became possible …, when the spacecraft was able to fly between the rings and the planet 22 times.

inferred from the dozen or so spiral density and bending waves currently seen in the rings that have been identified as being driven by mass fluctuations inside the planet (see section entitled Gravitational Processes). Nevertheless, it can be concluded with confidence that the ring mass is probably less than the Voyager-era estimate to within the uncertainty, see Section 3.2 Instruments Science Results chapter entitled RSS, and Iess et al. [2019]. A total ring mass even as large as 0.8 Mimas masses is regarded as unlikely, and the nominal value is 0.4 Mimas masses. While RSS has been as yet unable to obtain a radial profile of surface mass density, there is a clue from CIRS thermal models that the central B-ring region called B3 (105000–110000 km) is actually a quite sharply bounded annulus containing 2–3 times the surface mass density of the rest of the B-ring [Reffet et al. 2015].

Composition of Rings from Ring Ejecta

The AO mission provided for no direct, in situ measurement of main ring particle composition; it was planned to rely on remote observations by VIMS and CIRS, and eventually RADAR 2.2 cm radiometry, sensing the non-icy component of ring material (see section entitled Ring Particle Composition and Size). Unfortunately, no unambiguous compositional signatures of any materials besides water ice were seen by VIMS, UVIS, or ISS; and other instruments such as CIRS and RADAR could only constrain the amount of non-icy material in a nonspecific way. Fortunately, in the GF orbits, when Cassini crossed the ring plane inside of the D-ring (and indeed skimmed through the planet's tenuous upper atmosphere) synergistic, dedicated in situ observations by CDA, INMS, MIMI, and RPWS hit pay dirt.

CDA detected grains at a variety of vertical distances above the rings, with varying silicate/ice fraction [Hsu et al. 2018]. The Fe/Si ratio suggested low-Fe silicates. The order-unity silicate/ice ratio in material detected by CDA (primarily at high latitudes) is far higher than seen in the main rings or even the more polluted C-ring, and suggests that detected grains have been stripped of most of their ice before detection, perhaps by photosputtering [Hsu et al. 2018], but this remains an active area of research. No evidence was found for free iron or FexOy compounds (candidates for reddening the rings)—see section entitled Composition (Remote Sensing) and Cuzzi et al. [2009] for a review and discussion—even though their presence had been suggested in true interstellar grains detected by CDA [Altobelli et al. 2016]. CDA observations of organics are expected to be limited to large grains, which were rare because the dust abundance at the radii of ring plane crossings was much lower than had been (conservatively) estimated from spacecraft hazard studies, and most of the detected grains were too tiny to get good mass spectra in the presence of known carbon contamination of CDA. For the larger grains, CDA can say that the concentration of organics is low in any single detected grain, compared to the amount of ice or silicate. Nevertheless, the data are still being analyzed and new results along these lines are anticipated—see, for instance, Hsu et al. [2018], and Section 3.2 Instruments Science Results chapter entitled CDA.

MIMI detected an equatorial layer of 4–5 nm radius grains with vertical thickness of a few thousand km [Mitchell D. et al. 2018] blending into the very rare upper atmosphere of Saturn. These

tiny grains plausibly derive from the even flatter D-ring and drift inwards under gas drag while spreading vertically. They are too small to pick up much charge, so orbit at nearly Keplerian speeds, obtaining their few-thousand km vertical thickness by scattering collisions with differentially rotating exospheric H atoms. MIMI could not determine the composition of these grains directly, but estimates their mass flux into the atmosphere at 5 kg/s [Mitchell et al. 2018] (and Section 3.2 Instrument Science Results chapter entitled MIMI).

Meanwhile, as Cassini skimmed through the very rarified upper atmosphere on the GF orbits closest to Saturn, INMS detected strong signals due to a very wide range of masses, up to their limit at 100 amu [Waite et al. 2018; Perry et al. 2018]. The abundance of these molecules actually decreased downwards into Saturn, so they are entering from above, not diffusing up from depth. The overall pattern observed is roughly dominated by multiples of carbon atoms, up to C6, but given the likelihood that large molecules fragment into smaller ones within the INMS chamber prior to actually being sampled, detailed inferences require a complex deconvolution process [Waite et al. 2018; Miller et al. 2019]. INMS is unable to detect nonvolatile material like iron or silicates, and is even subject to underestimation of H_2O. The good agreement between the INMS latitudinal signal strength and the thickness of the MIMI 4–5 nm particle layer suggests that the INMS compositions refer to impact fragments of the MIMI particles. Also seen in the INMS spectra are N and O; however, the complexity of the deconvolution leaves some ambiguity about whether the O, N (and even some of the C) were carried as part of the organics or in smaller molecules like NH_3 or CH_4 [Waite et al. 2018; Perry et al. 2018; Miller et al. 2019]. For comparison, Cassini VIMS observations see no CH_4 or CO_2 [Cuzzi et al. 2009] and STIS spectra see no NH_3 [Cuzzi et al. 2018b]. INMS estimated a total flux of these materials into Saturn's upper atmosphere, over a latitudinal band of 5–10° wide, that is about 1000 times larger than the MIMI estimate [Perry et al. 2018], and propose that it must be carried dominantly by particles of 1–2 nm radius, too small for MIMI to detect, but following roughly the same vertical distribution. This flux is so high that INMS suggests it is probably due to a flareup in the D-ring, perhaps due to recent activity in the D68 ringlet [Hedman et al. 2014b; Hedman and Showalter 2016; Hedman 2019].

Ring origin and age

The age of the rings has been debated since the Voyager era, when two general lines of argument arose suggesting they may be much younger than the solar system. These are described in more detail in several recent review chapters [Cuzzi et al. 2009, 2018a; Charnoz et al. 2009]. First, angular momentum transfer by spiral density waves between the rings and the inner moons should quickly collapse the A-ring and spin the close ringmoons outwards, a tidal effect like our own Earth-moon tidal interaction [Goldreich and Tremaine 1982], see also Poulet and Sicardy [2001] or Charnoz et al. [2009] for loopholes. Second, pollution of the dominantly icy A-ring and B-ring, more than 90% ice, as known since pre-Voyager [Esposito et al. 1984; Orton et al. 2009], by dominantly non-icy meteoroid infall should darken them in much less than the age of the solar system [Doyle et al. 1989; Cuzzi and Estrada 1998; Elliott and Esposito 2011]. It had been argued, however, that the ring mass could be much larger than generally accepted during the Voyager era, because gravitational clumping and lack of sampling by spiral density waves of the most massive B-ring

might allow most of the mass to escape detection (see section entitled Gravitational Processes). Also, the meteoroid mass flux was very poorly known, and if it had been overestimated by an order of magnitude or so, the rings could remain unpolluted for the age of the solar system.

The combination of ring mass determined by RSS [Iess et al. 2019], and the extrinsic meteoroid mass flux measured by CDA [Kempf et al. 2019] (see section entitled The Extrinsic (Interplanetary) Mass Flux) at last allows us to constrain the ring age to be less than 250 million years or so (observational and model-based uncertainties remain), i.e., no older than the dinosau [O'Donoghue et al. 2019]. If we must reluctantly relinquish our otherwise physically plausible primordial ring origin scenarios, at least there is one plausible recent origin scenario, related to a dynamical instability incurred 100 million years ago by a stably evolving Saturn inner moon system [Cuk et al. 2016]. There are many current issues associated with connecting such an instability (near Rhea's orbit) and actual formation of a massive ring inside the Roche zone. However, it offers both an independently derived, recent age and also an indication why Saturn is the only giant planet to sport such a young, massive, icy ring. Constraints from cratering of icy moon surfaces and internal evolution will play an important role in testing the idea. There are also several Titan-related puzzles pointing to short timescales [Nixon et al. 2018]. A possibly important constraint is that the D/H ratio in the rings is similar to the regular icy moons and terrestrial values, while that of Phoebe is more comet-like [Clark et al. 2019]. The current implications that the rings are colored by organics, that there may be a silicate-rich rubble belt buried within the C-ring (see section entitled Composition (Remote Sensing)), and even the dark, enigmatic G-ring parent Aegaeon [Hedman et al. 2011a] provide important constraints as well.

Ring composition (RN1b) - ringmoons

Determines the composition of the close-in ringmoons as targets of opportunity. This is discussed in detail in Section 3.1 Discipline Science Results chapter entitled Icy Satellites.

Ring structure (RN1c) – high resolution and composition

Determines structural and compositional variations at high resolution across selected ring features of greatest interest, using remote and in situ observations.

A substantial number of new, dedicated observations were prioritized, integrated, and implemented to make use of the unique, up-close-and-personal geometry of Cassini's RG and GF orbits to address radial structure, meaning on scales larger than the vertical thickness. Also, a large number of ISS 8–15 filter color scans with 3–5 km radial resolution were integrated and successfully implemented well before the RG and GF orbits, to address compositional variations, over a large range of illumination and viewing angles, as well as different solar hour angles to assess the role of Saturnshine and the wavelength variation of ring particle phase functions.

Much higher spatial resolution is needed to assess fine scale structural variations. Recall that the unique SOI observations (400 m resolution) were sparsely sampled, were of the unlit face, and were taken at a large relative velocity requiring short exposures and producing noisy images. On

the other hand, the RG and GF orbits provided similar 100–300 m resolution on the lit face as well as of the unlit face, and at low phase angles, with the opportunity to use smear removal tracking. Moreover, one new kind of observation was enabled during the RG and GF orbits; active radar backscattering. Radar observations (from the ground) opened the modern era of Saturn's Rings research 40 years ago, but their sensitivity decreases as distance to the fourth power, so they only became feasible for Cassini in these very close-in geometries. The Radar team did carry out three active radar backscattering radial profiles with the potential to reach several km radial resolution, but reduction of this sort of data has not been previously done by the team and is still in progress (see Section 3.2 Instruments Science Results chapter entitled RADAR). Indeed, as of this writing, a number of observations taken on the RG and GF orbits remain in the early stages of analysis. However, an overview of high resolution observations by ISS, VIMS, UVIS, and CIRS may be found in Tiscareno et al. [2019].

Ring microstructure (RN2a)

Conducts in-depth studies of ring microstructure such as self-gravity wakes, which permeate the rings.

Microstructure has the connotation of structure comparable in scale to the ring vertical thickness (see section entitled Gravitational Processes). During the CSM, a number of exceptionally high radial resolution scans were implemented of the lit and unlit faces, using smear removal tracking (the so-called SUPERHRES scans) and targeted observations of, for instance, the Keeler gap in the vicinity of Daphnis, the C-ring plateaus, and other specific regions of interest. Spatial clumping, of several different types and on scales still larger than the expected self-gravity wakes, is widely seen in images with these sub-km resolutions [Tiscareno et al. 2019a]. A number of specially designed Turnaround stellar occultations were prioritized and included; these are chord occultations in which the path of the star becomes tangent to the orbital direction at some radius. The implication is that radial stellar velocity vanishes and ultra-high radial resolution can be obtained, along with very good tangential resolution. Finally, the technique of variance analysis 4 has been widely applied and a variety of interesting differences seen from place to place. This sort of analysis is only getting underway [Colwell et al. 2018].

New ring structures (RN2b)

Performs focused studies of the evolution of newly discovered propeller objects. Extend to studies of streaky plateau structure.

A dedicated campaign to image selected giant propellers (> 1 km size) as often as possible was conducted over the last five years of the mission. This campaign yielded several hundred images that successfully targeted propellers, with rich sampling in time. Ongoing analysis of these images—for example, see section entitled Ring-Satellite Interaction) finds excursions from Keplerian orbit of diverse kinds, including both gradual trends and sharp changes of direction. In the RG orbits, three giant propellers were specifically targeted for close-flyby imaging, which

successfully revealed their detailed structure. Also in the RG orbits, high-resolution images of the Propeller Belts yielded the first full view of a size distribution in which the largest propellers are 4× to 5× larger than the smallest [Tiscareno et al. 2019a]. In the GF orbits, images of the plateaus spectacularly confirmed previous suspicions of streaky texture, and further revealed sharp-edged belts of textures (some streaky, some clumpy) at other locations in the main rings [Tiscareno et al. 2019b]. Most of these data encompass both the lit and unlit faces of the rings, and are still under reduction and analysis.

Saturn System Science Results

The possibility of young rings now has broadened to the possibility of a young inner icy moon (and ring) system. The evection resonance theory of Cuk et al. [2016] not only independently arrives at a similar timescale as ring ages, but also points to Saturn as the most likely planet to incur such a fate. More studies of the icy moon surfaces (especially cratering statistics) are needed to constrain the validity of this hypothesis, and the composition of the moons and rings needs to be taken into account together.

Along these lines, results obtained through the study of rings have led us to a new understanding of the deep interior of Saturn. The discipline, now known as Kronoseismology, is in its infancy, and has led to the suggestion of a diffuse core boundary and rapidly changing internal structure at Saturn, see section entitled Gravitational Processes. Recent results have even shown that the elusive deep interior rotation period of the planet can be determined very precisely by matching internal structure predictions with spiral waves seen in the C-ring [Mankovich et al. 2019].

CDA also detected 46 grains coming from the Interstellar Flux stream (its velocity apex or ram direction is known from the velocity of the solar system through the local diffuse Interstellar medium) and constrained their composition [Altobelli et al. 2016]. This profoundly important in situ determination of the composition of interstellar medium (ISM) grains complements and informs often ambiguous remote sensing determinations, see section entitled Ring Age and Origin. The grains populating the diffuse ISM; those detected here and the most easily studied by remote sensing, include Mg-rich silicates and, perhaps, iron metal or oxides, but are depleted in sulfur. By comparison, the silicates detected by CDA during the GF orbits were also Mg-rich, but showed no evidence of companion Fe metal or oxides. The ISM grains were quite homogeneous, probably by repeated processing in the ISM by shocks and radiation. As these grains become embedded in the dark, dense, presolar parent cloud; they accumulate more volatile organics and ices (apparently some sulfur-bearing ices) before flowing into the forming solar system. However, their very refractory mix of silicates and metal would not be expected to change at the low temperatures of these clouds.

Non-Saturn-System Science Results

Cassini ISS took nearly 1200 images of the Jovian ring system during its 6-month encounter with Jupiter … .

Cassini ISS took nearly 1200 images of the Jovian ring system during its 6-month encounter with Jupiter [Porco et al. 2003]. These observations constitute the most complete data set on the ring taken by a single instrument, both in phase angle (0.5°–120° at seven angles) and wavelength (0.45–0.93 μm through eight filters). The optical depth and radial profile of the main ring are consistent with previous observations. No broad asymmetries within the ring were seen, but possible hints of 1000 km-scale azimuthal clumps were detected. Throop et al. [2004] combined the Cassini ISS and VIMS observations with those from Voyager, HST, Keck, Galileo, and groundbased telescopes, and fit the entire dataset using a photometric model including microscopic silicate dust grains and larger, long-lived parent bodies. Main ring optical depths for the large bodies, and the dust, of about 1–5 × 10^{-6}, respectively, were obtained, and the grains appear to be nonspherical. The larger bodies must be very red between 0.4–2.5 μm wavelengths, and may have absorption features near 0.8 and 2.2 μm.

Unsolved Problems Suitable for Ongoing Research and Future Missions

Figure RINGS-2 shows a montage of views displaying Saturn's main rings structure.

Why is the interior of Saturn different from that of Jupiter (as seen by the RSS gravity passes) and, why are the mass irregularities inferred so different and so much larger than what are inferred from Kronoseismology spiral density and bending waves in the rings? Are these differences tied to the faster tidal evolution rates seen for the Saturnian moons than for the Jovian moons (the so-called larger Q for Jupiter than for Saturn)? What are the embedded mass concentrations responsible for the tesseral spiral density waves that rotate at harmonics of Saturn's spin rate, and moreover change with time?

The ring mass and in particular its radial distribution were not as well constrained as hoped, because of unexpected internal structure within Saturn. Only a total ring mass could be determined, and the B-ring component inferred by backing out the already very well-known A-ring and C-ring masses (from spiral density waves). This remaining uncertainty provides an opportunity for a future mission to use repeated close gravitational flybys to separate out and fully understand the apparently unusual and intriguing internal structure of the planet, from the radial mass distribution within the rings, hopefully at a few hundred km radial resolution even, and to determine which parts of the opaque B-ring actually hold how much of the mass. Better radial mass resolution would be useful in the C-ring also, because the possibility that the middle C-ring hides a fossil silicate rubble belt has implications for ring origin; it is currently constrained by a small handful of surface mass densities. There is some evidence that the visual wavelength

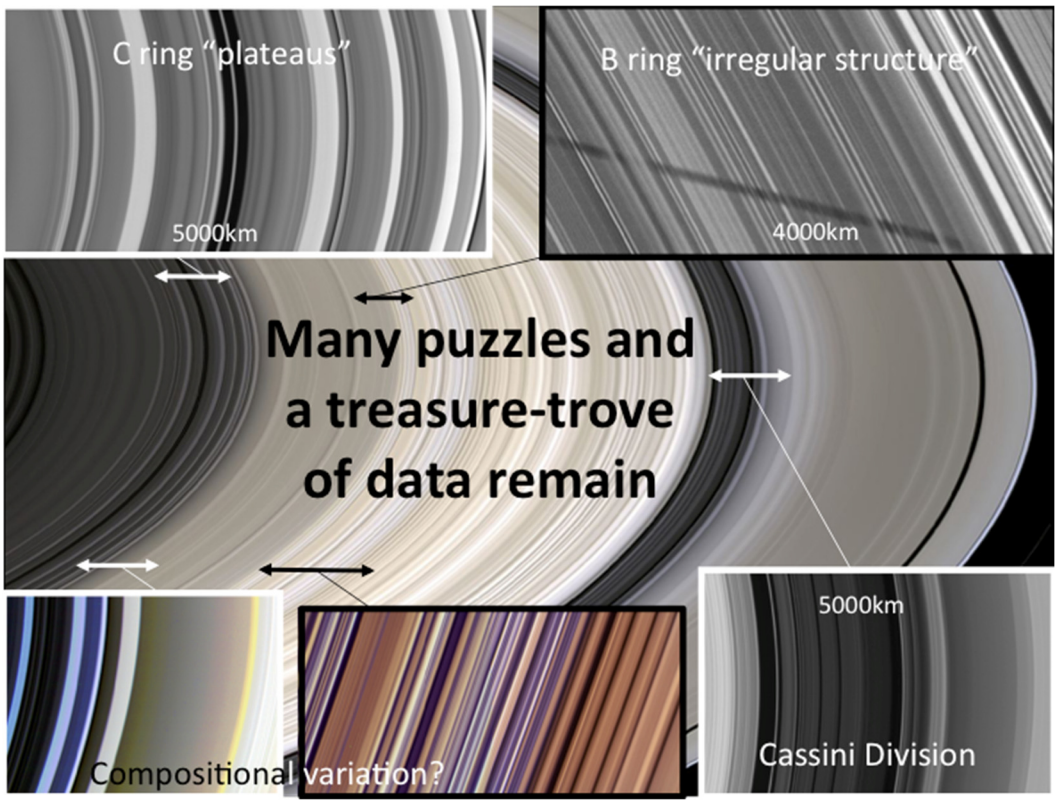

Figure RINGS-2: A montage of still-puzzling structure. A mosaic view of Saturn's main rings is shown in the central panel. Certain selected regions are indicated by double-header arrows, and by close-up images shown as insets.

spectra of the central C-ring differ from the otherwise similar Cassini Division; might this be another clue regarding a buried silicate belt?

The smooth, undulating 80 km scale irregular structure in the inner B-ring may be related to ballistic transport, but the array of finer-to-coarser scale structure in the middle and outer B-ring seems to be something different. Could it be some form of viscous overstability, operating at longer wavelengths than models show, and possibly coupling to the even larger scale azimuthal B-ring edge variations? In the region between 100,000–104,500 km, radio and stellar occultations both see successions of very sharp transitions between large and very large optical depth, for which no explanations exist. At the time of this writing, RSS occultations of the very densest B-ring regions, taken at the largest ring opening angles where they would be most likely to be even partially transparent, have not been analyzed or released, but are eagerly anticipated.

The outer C-ring hosts a series of 5–8 plateau features in optical depth, nearly symmetrically arrayed about the Maxwell gap which is now known to be caused by a 2:1 resonance with the strongest planetary internal vibration mode [Marley and Porco 1993; French et al. 2016b; Fuller 2014]; the reason why a dense, elliptical m = 1 ringlet dominates the gap, apparently caused by an m = 2 resonance, is not understood. A similar situation occurs at a Titan resonance in the C-ring, but that is an m = 1 resonance. The plateaus do not have any special association with resonances

from known or predicted planetary internal modes [Marley 2014]. They are odd in that their appearance as features is due primarily to locally abrupt changes in particle size distribution rather than surface mass density, see section entitled Size Distribution, and the following paragraphs. Moreover, ultra-high resolution Cassini images reveal a novel and unique streaky structure in the plateaus that is not understood [Tiscareno et al. 2019a].

Why is there a Cassini Division and why are there no embedded moonlets clearing its several empty gaps? It has been suggested that weak perturbations from the fluctuating B-ring edge might play a role [Hedman et al. 2010b]. Presumably the Cassini Division was originally cleared by a powerful Mimas 2:1 spiral density wave, at a time when the rings were continuous through the region [Baillié et al 2019] , but how did that early, vigorous evolution lead to today's quiet, banded structure? And, how are the moonlet-free C-ring gaps formed?

In the A-ring, a million propeller objects populate three distinct radial belts. Are these objects transient clumps that emerge from the background material with low, but finite probability and then disperse again? Giant propellers (found only outside the Encke gap) seem especially hard to create by spontaneous, or triggered formation. Gravitational encounters with smaller masses seem to explain their wandering behavior, but the mass clumps needed are larger than the largest ring particles and even typical self-gravity wakes. There are a few propeller objects in the B-ring, but their locations and abundances have not been well characterized. What else could be hiding in the densest parts of the B-ring? What causes the ghost gaps in the C-ring and outer Cassini Division?

In the F-ring, telltale signatures of embedded, relatively large objects are seen preferentially in strands where they are maximally compressed by Prometheus. If the semi-major axes of these newly created objects lie outside the stable true core (see section entitled F-ring), they will develop chaotic orbital perturbations, diffusing away from their formation location as their eccentricity increases, and ultimately recolliding sporadically with the F-ring core. Cycles of such activity may be expected (and there is some evidence from comparing Voyager and Cassini), but no systematic assessment has been obtained. Meanwhile, even the most recent hypothesis for the stability of the F-ring true core cannot explain the stable precession of dozens of separated arcs as a single, well defined ellipse. Could the (mostly unconstrained) mass of the F-ring be playing a role?

The systematic increase of the redness of the rings inwards across the B-ring remains a puzzle. In situ observations (albeit in the D-ring) seem to favor large organic molecules, polycyclic aromatic hydrocarbons (PAHs) or fragments of tholins, possibly containing N and maybe even O, as the UV absorber responsible for the ring redness. These red organics seem to be intrinsic to the dominant icy material. Whether or not organics also explain the weaker UV absorption seen in most of the icy moons will be an important clue regarding ring origin scenarios; such as recent ones that connect their origin to a moderately recent collisional erosion/destruction of pre-existing, mature, differentiated icy moons. Can organic material remain associated with liquid water when a moon differentiates, and remain with it when it freezes?

Unexplained microstructure is seen in many places across the rings, at optical depths large and small, in late, high-resolution images which have resolution even better than those taken at SOI, … .

Color and brightness variations within the rings on tens to hundreds of km scale have been interpreted as small-scale, optical-depth dependent regolith grain size variations, but models capable of treating the difficult ring radiative transfer problem have yet to be deployed in compositional analyses. That is, secondary optical-depth dependent effects (like collisional packing or smoothing of particle surfaces) may change the particle phase functions, or volume density effects may change the layer scattering function. Much more analysis needs to be done with more sophisticated, nonclassical radiative transfer models, fitting observations over wide ranges of illumination and viewing geometry, as well as assessing wider ranges of wavelength simultaneously, to understand the situation before compositional implications can be derived with confidence. Shadowing on the surely very ragged ring particle surfaces needs to be studied [Cuzzi et al. 2017]. Also on the subject of radiative transfer models, Cassini's three high-radial-resolution active radar backscattering scans require new models for their interpretation that can adequately treat coherent backscattering.

Unexplained jumps in particle size distribution are seen at a number of places in the rings where sharp edges appear in optical depth, but across these edges there are only small (or no) contrasts in surface mass density. Basically, this means the features are caused by abrupt changes in particle size distribution. The inner edge of the A-ring, where it transitions to the Cassini Division, is one such place. The series of C-ring plateaus, nearly symmetrically surrounding the Maxwell gap (which is known to be associated with a 2:1 resonance with a mode inside Saturn) are like that as well. What causes this effect? Why do the slopes and minimum or maximum sizes in generally powerlaw size distributions of ring particles vary from place to place? Are most particles porous throughout or do they conceal dense, solid cores?

Unexplained microstructure is seen in many places across the rings, at optical depths large and small, in late, high-resolution images which have resolution even better than those taken at SOI, as well as combinations of lit and unlit face geometries, lower smear, and higher signal to noise ratio [Tiscareno et al. 2019a]. The texture can change rather quickly with radius and is not always related to optical depth changes.

The process actually responsible for the initial formation of spokes; whether it be bursts of ionizing radiation from planetary superstorms, magnetic field instabilities, or impacts, remains unclear.

The Ballistic transport process usually believed to explain the sharp inner edges of the A-ring and B-ring, and hypothesized to explain the C-ring plateaus, has been modeled assuming the boundaries of these features manifested jumps in surface mass density without particle size changes, and we now know the underlying surface mass density is only slowly varying while the particle size changes abruptly. How do these new realizations affect the models? Could the ejection

velocity change from place to place, depending on the nature of the local particle regoliths? How will the results change under new assumptions about meteoroid impact flux and dynamical population? The theory of ring pollution and restructuring by meteoroid bombardment and ballistic transport needs to be tested more carefully against other structures and compositional profiles, and revised to capture more realistic impact outcomes and newly constrained incoming meteoroid fluxes. Matching radial scans of ring color and spectral reflectance with models of compositional evolution must incorporate new understanding about ring surface mass density, particle size, and viscosity. Inclusion of regolith thermal inertias would provide another handle on how particle surfaces respond to meteoroid bombardment.

More sophisticated models of impact chemistry and radiation chemistry are needed; both in micrometeoroid impacts on ring particles, possibly resulting in some C-O chemistry, and by nm-size grain impacts into the INMS entry chamber. INMS sees a variety of molecules (CH_4, CO_2, and NH_3 in particular) that are not evident in VIMS or HST-STIS spectra of the rings. Are some of these created in hypervelocity impacts, transforming absorbing carbon compounds into volatiles or transparent ices? If so (or if not) this would have implications for ring pollution and inferred ring age. How does the water ice throughout the rings remain crystalline given constant radiation and meteoroid bombardment? VIMS spectral and occultation observations strongly support crystalline ice.

Explanation for the geologically recent formation of the rings: We now have a new set of constraints, and even an appealing theoretical hypothesis to explore; however, we are still lacking a complete understanding as to how the rings formed in their current location, within Saturn's Roche limit, from a differentiated icy object with a trace, intimately mixed organic component, 250 million years ago, even given disruptive collisions near the current orbit of Rhea. Observations and interpretation of icy moon surfaces can contribute meaningful constraints.

CONCLUSION

This short review can in no way capture the depth and complexity of the analysis that has gone into every one of the incomplete list of ~200 publications cited here, each of them several years work for multiple scientists. Each of these papers has contributed one critical and unique stone to the edifice of knowledge we now possess about the rings of Saturn; stones all formed from bits returned by Cassini's spectacular 13-year mission. Nor can it adequately convey the even larger and deeper, still unanalyzed and uninterpreted amount of data so thoughtfully conceived, passionately argued for, painstakingly planned, obtained, carefully calibrated, and stored in the Planetary Data System that awaits the attention of future generations of ring scientists. However, we hope it can provide an idea of the scope of where we stand today, and hints at future directions of research. Even this summary would be different if it were written a year from now. The Cassini Rings Discipline Working Group has nothing but admiration and deep appreciation for the dedication of the hundreds of engineers and dozens of managers at Jet Propulsion Laboratory (JPL) who made this mission possible, some of whom may be lucky enough to return to Saturn on a future mission and help answer these outstanding questions.

ACRONYMS

Note: For a complete list of Acronyms, refer to Cassini Acronyms – Attachment A.

AO	Announcement of Opportunity
CAPS	Cassini Plasma Spectrometer
CDA	Cosmic Dust Analyzer
CIRS	Composite Infrared Spectrometer
CSM	Cassini Solstice Mission
FOV	field-of-view
GF	Grand Finale
HST	Hubble Space Telescope
INMS	Ion and Neutral Mass Spectrometer
IR	infrared
ISM	interstellar medium
JPL	Jet Propulsion Laboratory
KBO	Kuiper Belt object
MAPS	Magnetospheres and Plasma Science
MIMI	Magnetospheric Imaging Instrument
NIR	near-IR
PAH	polycyclic aromatic hydrocarbon
PDS	Planetary Data System
RADAR	Titan Radar Mapper
RG	Ring-Grazing
RSS	Radio Science Subsystem
RWG	Ring Working Group
SED	Saturn Electrostatic Discharge
SKR	Saturn Kilometric Radiation
SOI	Saturn Orbit Insertion
STIS	Space Telescope Imaging Spectrograph
TM	Traceability Matrix
UV	ultraviolet
UVIS	Ultraviolet Imaging Spectrograph
VIMS	Visual and Infrared Imaging Spectrometer
WP	water products

REFERENCES

Disclaimer: The partial list of references below correspond with in-text references indicated in this report. For all other Cassini references, refer to Attachment B – References & Bibliographies; Attachment C – Cassini Science Bibliographies; the sections entitled References contributed by individual Cassini instrument and discipline teams located in Volume 1 Sections 3.1 and 3.2 Science Results; and other resources outside of the Cassini Final Mission Report.

Albers, N., M. Sremčević, J. E. Colwell, L. W. Esposito, (2012), Saturn's F-ring as seen by Cassini UVIS: Kinematics and statistics, Icarus, 217, 367−388.

Altobelli, N., F. Postberg, K. Fiege, M. Trieloff, H. Kimura, V. J. Sterken, H.-W. Hsu, J. Hillier, N. Khawaja, G. Moragas-Klostermeyer, J. Blum, M. Burton, R. Srama, S. Kempf, E. Gruen, (2016), Flux and composition of interstellar dust at Saturn from Cassini's Cosmic Dust Analyzer, Science, 352, 312−318.

Altobelli, N., L. Spilker, S. Pilorz, C. Leyrat, S. Eddgington, B. Wallis, A. Flandes, (2009), Thermal phase curves observed in Saturn's main rings by Cassini-CIRS: Detection of an opposition effect?, Geophysical Research Letters 36, L10105, doi: 10.1029/2009gl038163.

Altobelli, N., L. Spilker, S. Pilorz, S. Brooks, S. Edgington, B. Wallis, M. Flasar, (2007), C-ring fine structures revealed in the thermal infrared, Icarus, 191, 2, 691−701, doi: 10.1016/j.icarus.2007.06.014.

Attree, N. O., C. D. Murray, G. A. Williams, N. J. Cooper, (2014), A survey of low-velocity collisional features in Saturn's F-ring, Icarus, 227, 56−66.

Attree, N. O., C. D. Murray, N. J. Cooper, G. A. Williams, (2012), Detection of low-velocity collisions in Saturn's F-ring, The Astrophysical Journal Letters, vol. 755, no. 2, doi: 10.1088/2041-8205/755/2/L27.

Baillié, K., B. Noyelles, V. Lainey, S. Charnoz, G. Tobie, (2019), Formation of the Cassini Division-I, Shaping the rings by Mimas inward migration, Monthly Notices of the Royal Astronomical Society, 486, 2933−2946, doi: 10.1093/mnras/stz548.

Baillié, K., J. E. Colwell, L. W. Esposito, M. C. Lewis, (2013), Meter-sized moonlet population in Saturn's C-ring and Cassini Division, The Astronomical Journal, vol. 145, no. 6, doi: 10.1088/0004-6256/145/6/171.

Baillié, K., J. E. Colwell, J. J. Lissauer, L. W. Esposito, M. Sremčević, (2011), Waves in Cassini UVIS stellar occultations, 2, The C-ring, Icarus, 216, 292−308.

Becker, T. M., J. E. Colwell, L. W. Esposito, N. O. Attree, C. D. Murray, (2018), Cassini UVIS solar occultations by Saturn's F-ring and the detection of collision-produced micron-sized dust, Icarus, 306, 171−199.

Becker, T. M., J. E. Colwell, L. W. Esposito, A. D. Bratcher, (2016), Characterizing the particle size distribution of Saturn's A-ring with Cassini UVIS occultation data, Icarus, 279, 20−35.

Beurle, K., C. D. Murray, G. A. Williams, M. W. Evans, N. J. Cooper, C. B. Agnor, (2010), Direct Evidence for gravitational instability and moonlet formation in Saturn's rings, The Astrophysical Journal, 718, L176-L180.

Borderies, N., P. Goldreich, S. Tremaine, (1985), A granular flow model for dense planetary rings, Icarus, 63, 406−420.

Bradley, E. T., J. E. Colwell, L. W. Esposito, (2013), Scattering properties of Saturn's rings in the far ultraviolet from Cassini UVIS spectra, Icarus, 225, 726−739.

Bradley, E. T., J. E. Colwell, L. W. Esposito, J. N. Cuzzi, H. Tollerud, L. Chambers, (2010), Far ultraviolet spectral properties of Saturn's rings from Cassini UVIS, Icarus 206, 458−466.

Bromley, B. C. and Kenyon, S. J., (2013), Migration of small moons in Saturn's rings, The Astrophysical Journal, vol. 764, no. 2.

Burns, J. A., L. E. Schaffer, R. J. Greenberg, M. R. Showalter, (1985), Lorentz resonances and the structure of the Jovian ring, Nature, 316, 115−119.

Burns, J. A., M. R. Showalter, G. E. Morfill, (1984), The ethereal rings of Jupiter and Saturn, In Planetary rings, (eds.) R. Greenberg, A. Braphic, (A85-34401 15-88), University of Arizona Press, Tucson, AZ, 200−272.

Chambers, L. S., J. N. Cuzzi, E. Asphaug, J. Colwell, S. Sugita, (2008), Hydrodynamical and radiative transfer modeling of meteoroid impacts into Saturn's rings, Icarus, 194, 623−635.

Chancia, R. O., M. M. Hedman, S. W. H. Cowley, G. Provan, S. -Y. Ye, (2019), Seasonal structures in Saturn's dusty Roche Division correspond to periodicities of the planet's magnetosphere, Icarus, vol. 330, pp. 230−255, doi: 10.1016/j.icarus.2019.04.012.

Charnoz, S., R. M. Canup, A. Crida, L. Dones, (2018), The Origin of Planetary Ring Systems, Chapter 18, In Planetary Rings, (eds.) M. Tiscareno, C. Murray, Cambridge University Press pp. 515−536, doi: 10.1017/9781316286791.018.

Charnoz, S., J. Salmon, A. Crida, (2010), The recent formation of Saturn's moonlets from viscous spreading of the main rings, Nature, 465, 752−754.

Charnoz, S., L. Dones, L. W. Esposito, P. R. Estrada, M. M. Hedman, (2009), Origin and Evolution of Saturn's Ring System, Chapter 17, In Saturn from Cassini-Huygens, (eds.) M. K. Dougherty, L. W. Esposito, S. M. Krimigis, Springer, Dordrecht, pp. 537–575, doi: 10.1007/978-1-4020-9217-6_17.

Charnoz, S., (2009), Physical collisions of moonlets and clumps with the Saturn's F-ring core, Icarus, 201, 191−197.

Charnoz, S., C. C. Porco, E. Déau, A. Brahic, J. N. Spitale, G. Bacques, K. Baillié, (2005), Cassini Discovers a Kinematic Spiral Ring Around Saturn, Science, 310, 1300−1304.

Ciarniello, M., G. Filacchione, E. D'Aversa, F. Capaccioni, P. D. Nicholson, J. N. Cuzzi, R. N. Clark, M. M. Hedman, C. M. Dalle Ore, P. Cerroni, C. Plainaki, L. J. Spilker, (2019), Cassini-VIMS observations of Saturn's main rings II: A spectrophotometric study by means of Monte Carlo ray-tracing and Hapke's theory, Icarus, 317, pp. 242−265, doi: 10.1016/j.icarus.2018.07.010.

Clark, R. N., R. H. Brown, D. P. Cruikshank, G. A. Swayze, (2019), Isotopic ratios of Saturn's rings and satellites: Implications for the origin of water and Phoebe, Icarus, 791−802, doi: 10.1016/j.icarus.2018.11.029.

Clark, R. N., D. P. Cruikshank, R. Jaumann, R. H. Brown, K. Stephan, C. M. Dalle Ore, K. E. Livo, N. Pearson, J. M. Curchin, T. M. Hoefen, B. J. Buratti, G. Filacchione, K. H. Baines, P. D. Nicholson, (2012), The surface composition of Iapetus: Mapping results from Cassini VIMS, Icarus, 218, 831−860.

Colwell, J. E., L. W. Esposito, J. H. Cooney, (2018), Particle sizes in Saturn's rings from UVIS stellar occultations 1, Variations with ring region, Icarus, 300, 150−166.

Colwell, J. E., P. D. Nicholson, M. S. Tiscareno, C. D. Murray, R. G. French, E. A. Marouf, (2009), The Structure of Saturn's Rings, Chapter 13, In Saturn from Cassini-Huygens, (eds.) M. K. Dougherty, L. W. Esposito, S. M. Krimigis, Springer, Dordrecht, pp. 375−412, doi: 10.1007/978-1-4020-9217-6_13.

Colwell, J. E., L. W. Esposito, M. Sremčević, G. R. Stewart, W. E. McClintock, (2007), Self-gravity wakes and radial structure of Saturn's B-ring, Icarus, 190, 127−144.

Colwell, J. E., L. W. Esposito, M. Sremčević, (2006), Self-gravity wakes in Saturn’s A-ring measured by stellar occultations from Cassini, Geophysical Research Letters, 33, L07201.

Connerney, J. E. P. and J. H. Waite, (1984), New model of Saturn's ionosphere with an influx of water from the rings, Nature, 312, 136−138.

Cooper, N. J., C. D. Murray, S. Renner, (2017), F-ring Objects, Presented at Cassini End of Mission Project Science Group (PSG), Pasadena, CA, September 16, 2017.

Cooper, N. J., C. D. Murray, G. A. Williams, (2013), Local variability in the orbit of Saturn's F-ring, The Astronomical Journal, vol. 145, no. 6, doi: 10.1088/0004-6256/145/6/161.

Crida, A., J. C. B. Papaloizou, H. Rein, S. Charnoz, J. Salmon, (2010), Migration of a moonlet in A-ring of solid particles: Theory and application to Saturn's propellers, The Astrophysical Journal, 140, 944−953.

Ćuk, M., L. Dones, D. Nesvorný, (2016), Dynamical evidence for a late formation of Saturn’s Moons, The Astrophysical Journal, 820, 2, 97.

Cuzzi, J. N., G. Filacchione, E. A. Marouf, et al., (2018a), The Rings of Saturn, Chapter 3, In Planetary Ring Systems, (eds.) M. Tiscareno and C. Murray, Cambridge University Press, pp. 51−92, doi: 10.1017/9781316286791.003.

Cuzzi, J. N., R.G. French, A. R. Hendrix, D. M. Olson, T. Roush, S. Vahidinia, (2018b), HST-STIS spectra and the redness of Saturn's rings, Icarus, 309, 363−388.

Cuzzi, J. N., E. A. Marouf, R. G. French, R. A. Jacobson, C. D. Murray, N. J. Cooper, (2018c), Saturn’s F-ring is shepherded by Prometheus, Science Advances, in review.

Cuzzi, J. N., L. B. Chambers, A. R. Hendrix, (2017), Rough surfaces: Is the dark stuff just shadow? Icarus, 289, 281−294.

Cuzzi, J. N., A. D. Whizin, R. C. Hogan, A. R. Dobrovolskis, L. Dones, M. R. Showalter, J. E. Colwell, J. D. Scargle, (2014) ,Saturn’s F-ring core: Calm in the midst of chaos, Icarus, 232, 157−175.

Cuzzi, J. N., J. A. Burns, S. Charnoz, R. N. Clark, J. E. Colwell, L. Dones, L. W. Esposito, G. Filacchione, R. G. French, M. M. Hedman, S. Kempf, E. A. Marouf, C. D. Murray, P. D. Nicholson, C. C. Porco, J. Schmidt, M. R. Showalter, L. J. Spilker, J. N. Spitale, R. Srama, M. Sremčević, M. S. Tiscareno, J. Weiss, (2010), An evolving view of Saturn's dynamic rings, Science, 327, 1470−1475.

Cuzzi, J., R. Clark, G. Filacchione, R. French, R. Johnson, E. Marouf, L. Spilker, (2009), Ring Particle Composition and Size Distribution, Chapter 15, In Saturn from Cassini-Huygens, (eds.) M. K. Dougherty, L. W. Esposito, S. M. Krimigis, Springer, Dordrecht, pp. 459−509, doi: 10.1007/978-1-4020-9217-6.

Cuzzi, J. N. and P. R. Estrada, (1998), Compositional evolution of Saturn's rings due to meteoroid bombardment, Icarus, 132, 1−35.

D'Aversa, E., G. Bellucci, P. D. Nicholson, M. M. Hedman, R. H. Brown, M. R. Showalter, F. Altieri, F. G. Carrozzo, G. Filacchione, F. Tosi, (2010), The spectrum of a Saturn ring spoke from Cassini/VIMS, Geophysical Research Letters, 37, 1.

Déau, E., L. Dones, L. Spilker, A. Flandes, K. Baillié, S. Pilorz, M. Showalter, M. El Moutamid, J. E. Colwell, (2019), Cassini CIRS and ISS opposition effects of Saturn's rings: 1, C-ring narrow or broad surge? Monthly Notices of the Royal Astronomical Society, vol. 489, Issue 2, pp. 2775–2791, doi: 10.1093/mnras/sty2587.

Déau, E., L. Dones, M. I. Mishchenko, R. A. West, P. Helfenstein, M. M. Hedman, C.C. Porco, (2018), The opposition effect in Saturn's main rings as seen by Cassini ISS: 4, Correlations of the surge morphology with surface albedos and VIMS spectral properties, Icarus, 305, 324−349.

Déau, E., (2015), The opposition effect in Saturn's main rings as seen by Cassini ISS: 2, Constraints on the ring particles and their regolith with analytical radiative transfer models, Icarus, 253, 311−345.

Déau, E., L. Dones, S. Charnoz, R. A. West, A. Brahic, J. Decriem, C. C. Porco, (2013), The opposition effect in Saturn's main rings as seen by Cassini ISS: 1, Morphology of phase functions and dependence on the local optical depth, Icarus, 226, 591−603.

Dougherty, M. K., H. Cao, K. K. Khurana, G. J. Hunt, G. Provan, S. Kellock, M. E. Burton, et al., (2018), Saturn's magnetic field revealed by the Cassini Grand Finale, Science, 362, 6410, doi: 10.1126/science.aat5434.

Doyle, L. R., L. Dones, J. N. Cuzzi, (1989), Radiative transfer modeling of Saturn's outer B-ring, Icarus, vol. 80, pp. 104−135, doi: 10.1016/0019-1035(89)90163−-2.

Durisen, R. H., P. W. Bode, J. N. Cuzzi, S. E. Cederbloom, B. W. Murphy, (1992), Ballistic transport in planetary ring systems due to particle erosion mechanisms II: Theoretical models for Saturn's A- and B-ring inner edges, Icarus, 100, 364−393.

Durisen, R. H., N. L. Cramer, B. W. Murphy, J. N. Cuzzi, T. L. Mullikin, S. E. Cederbloom, (1989), Ballistic transport in planetary ring systems due to particle erosion mechanisms I: Theory, numerical methods, and illustrative examples, Icarus, 80, 136−166.

El Moutamid, M., P. D. Nicholson, M. M. Hedman, P. J. Gierasch, J. A. Burns, R. G. French, (2016a), Tesseral resonances in the rings of Saturn, American Astronomical Society (AAS),

Division on Dynamical Astronomy (DDA), meeting 47, id. 400.05, Vanderbilt University, Nashville, TN, May 22−26, 2016.

El Moutamid, M., M. M. Hedman, P. D. Nicholson, P.J. Gierasch, J. A. Burns, (2016b), Evidence of differential rotation inside Saturn from waves of its rings, American Astronomical Society (AAS), Division for Planetary Sciences (DPS), meeting 48, id. 114.0, Pasadena, CA, October 16−21, 2016.

El Moutamid, M., P. D. Nicholson, R. G. French, M. S. Tiscareno, C. D. Murray, M. W. Evans, C. M. French, M. M. Hedman, J. A. Burns, (2016c), How Janus' orbital swap affects the edge of Saturn's A-ring?, Icarus, 279, 125−140.

Elliott, J. P. and L. W. Esposito, (2011), Regolith depth growth on an icy body orbiting Saturn and evolution of bidirectional reflectance due to surface composition changes, Icarus, 2012, 268−274.

Elrod, M. K., W.-L. Tseng, A. K. Woodson, R. E. Johnson, (2014), Seasonal and radial trends in Saturn's thermal plasma between the main rings and Enceladus, Icarus, 242, 130−137.

Esposito, L. W., N. Albers, B. K. Meinke, M. Sremčević, P. Madhusudhanan, J. E. Colwell, R. G. Jerousek, (2012), A predator-prey model for moon-triggered clumping in Saturn's rings, Icarus, 217, 103−114.

Esposito, L. W., B. K. Meinke, J. E. Colwell, P. D. Nicholson, M. M. Hedman, (2008), Moonlets and clumps in Saturn's F-ring, Icarus, 194, 278−289.

Esposito, L. W., J. N. Cuzzi, J. B. Holberg, E. A. Marouf, G. L. Tyler, C. C. Porco, (1984), Saturn's rings-structure, dynamics, and particle properties, Saturn, 463−545.

Estrada, P. R., R. H. Durisen, H. N. Latter, (2018), Meteoroid bombardment and ballistic transport in planetary rings, Chapter 9, In Planetary Rings, (eds.) M. Tiscareno, C. Murray, Cambridge University Press, pp. 198−224, doi: 10.1017/9781316286791.009.

Estrada, P. R., R. H. Durisen, J. N. Cuzzi, D. A. Morgan, (2015), Combined structural and compositional evolution of planetary rings due to micrometeoroid impacts and ballistic transport, Icarus, 252, 415−439.

Ferrari, C., S. Brooks, S. Edgington, et al., (2009), Structure of self- gravity wakes in Saturn's A-ring as measured by Cassini CIRS, Icarus, 199, 145–153.

Filacchione, G., M. Ciarniello, F. Capaccioni, R. N. Clark, P. D. Nicholson, M. M. Hedman, J. N. Cuzzi, D. P. Cruikshank, C. M. Dalle Ore, R. H. Brown, P. Cerroni, N. Altobelli, L. J. Spilker, (2014), Cassini-VIMS observations of Saturn's main rings I: Spectral properties and temperature radial profiles variability with phase angle and elevation, Icarus, 241, 45−65.

Filacchione, G., F. Capaccioni, R. N. Clark, P. D. Nicholson, D. P. Cruikshank, J. N. Cuzzi, J. I. Lunine, R. H. Brown, P. Cerroni, F. Tosi, M. Ciarniello, B. J. Buratti, M. M. Hedman, E. Flamini, (2013), The radial distribution of water ice and chromophores across Saturn's System, The Astrophysical Journal, vol. 766, no. 2, doi: 10.1088/0004-637X/766/2/76.

Filacchione, G., F. Capaccioni, M. Ciarniello, R. N. Clark, J. N. Cuzzi, P. D. Nicholson, D. P. Cruikshank, M. M. Hedman, B. J. Buratti, J. I. Lunine, L. A. Soderblom, F. Tosi, P. Cerroni, R. H. Brown, T. B. McCord, R. Jaumann, K. Stephan, K. H. Baines, E. Flamini, (2012),

Saturn's icy satellites and rings investigated by Cassini-VIMS III: Radial compositional variability, Icarus, 220, 1064−1096.

Flandes, A., L. Spilker, R. Morishima, S. Pilorz, C. Leyrat, N. Altobelli, S. Brooks, S. G. Edgington, (2010), Brightness of Saturn's rings with decreasing solar elevation, Planetary and Space Science, 58, 1758–1765.

French, R. G., C. A. McGhee-French, P. D. Nicholson, M. M. Hedman, (2019), Kronoseismology III: Waves in Saturn's inner C-ring, Icarus, 319, pp. 599−626, doi: 10.1016/j.icarus.

French, R. G., P. D. Nicholson, C. A. McGhee-French, K. Lonergan, T. Sepersky, M. M. Hedman, E. A. Marouf, J. E. Colwell, (2016a), Noncircular features in Saturn's rings III: The Cassini Division, Icarus, 274, 131−162.

French, R. G., P. D. Nicholson, M. M. Hedman, J. M. Hahn, C. A. McGhee-French, J. E. Colwell, E. A. Marouf, N. J. Rappaport, (2016b), Deciphering the embedded wave in Saturn's Maxwell ringlet, Icarus, 279, 62−77.

French, R. S., S. K. Hicks, M. R. Showalter, A. K. Antonsen, D. R. Packard, (2014), Analysis of clumps in Saturn's F-ring from Voyager and Cassini, Icarus, 241, 200−220.

French, R. S., M. R. Showalter, R. Sfair, C. A. Argüelles, M. Pajuelo, P. Becerra, M. M. Hedman, P. D. Nicholson, (2012), The brightening of Saturn's F-ring, Icarus, 219, 181−193.

French, R. G., E. A. Marouf, N. J. Rappaport, C. A. McGhee, (2010), Occultation Observations of Saturn's B-ring and Cassini Division, The Astronomical Journal, 139, 1649−1667.

Fuller, J., J. Luan, E. Quataert, (2016), Resonance locking as the source of rapid tidal migration in the Jupiter and Saturn moon systems, Monthly Notices of the Royal Astronomical Society, 458, 3867−3879.

Fuller, J., (2014), Saturn ring seismology: Evidence for stable stratification in the deep interior of Saturn, Icarus, 242, 283−296.

Goldreich, P. and S. Tremaine, (1982), The dynamics of planetary rings, Annual Review of Astronomy and Astrophysics, 20, 249−283.

Goldreich, P. and S. Tremaine, (1980), Disk-satellite interactions, The Astrophysical Journal, 241, 425−441.

Gurnett, D. A., W. S. Kurth, G. B. Hospodarsky, A. M. Persoon, L. Xin, W. Farrell, A. Lecacheux, J.-E. Wahlund, (2004), Cassini Observations of Radio and Plasma Wave Phenomena Associated with the Saturn's Rings, Bulletin of the American Astronomical Society, vol. 36, p. 1067.

Harbison, R. A., P. D. Nicholson, M. M. Hedman, (2013), The smallest particles in Saturn's A- and C-ings, Icarus, 226, 1225−1240.

Hedman, M. M., P. D. Nicholson, R. G. French, (2019), Kronoseismology IV: Six Previously Unidentified waves in Saturn's middle C-ring, The Astronomical Journal, vol. 157, no. 1, doi: 10.3847/1538-3881/aaf0a6.

Hedman, M. M. and P. D. Nicholson, (2019), Axisymmetric density waves in Saturn's rings, Monthly Notices of the Royal Astronomical Society, 485, 13−29, doi: 10.1093/mnras/stz301.

Hedman, M. M., (2019), Bright clumps in the D68 ringlet near the end of the Cassini Mission, Icarus, 323, 62−75, doi: 10.1016/j.icarus.2019.01.007.

Hedman, M. M., F. Postberg, D. P. Hamilton, S. Renner, H.-W. Hsu, (2018a), Dusty Rings, Chapter 12, In Planetary Rings, (eds.) M. Tiscareno, C. Murray, Cambridge University Press, pp. 308−337, doi: 10.1017/9781316286791.012.

Hedman, M. M., P. D. Nicholson, M. El Moutamid, (2018b), Evidence for changes in Saturn's interior from structures in its rings, 49th Lunar and Planetary Science Conference, Houston, TX, March 19−23, 2018, LPI Contribution no. 2083, id. 1288.

Hedman, M. M., M. El Moutamid, P. D. Nicholson, (2017), Drifting waves in Saturn's C-ring, evidence for changes in Saturn's interior, American Astronomical Society (AAS), Division on Dynamical Astronomy (DDA) meeting 48, id. 401.03.

Hedman, M. M. and P. D. Nicholson, (2016), The B-ring's surface mass density from hidden density waves: Less than meets the eye?, Icarus, 279, 109−124.

Hedman, M. M. and M. R. Showalter, (2016), A new pattern in Saturn's D-ring created in late 2011, Icarus, 279, 155−165.

Hedman, M. M., J. A. Burns, M. R. Showalter, (2015), Corrugations and eccentric spirals in Saturn's D-ring: New insights into what happened at Saturn in 1983, Icarus, 248, 137−161.

Hedman, M, M. and C, C. Stark, (2015), Saturn's G- and D-rings provide nearly complete measured scattering phase functions of nearby debris disks, The Astrophysical Journal, vol. 811, no. 1, doi: 10.1088/0004-637X/811/1/67.

Hedman, M. M., P. D. Nicholson, H. Salo, (2014a), Exploring overstabilities in Saturn's A-ring using two stellar occultations, The Astronomical Journal, 148, 15, doi: 10.1088/0004-6256/148/1/15.

Hedman, M. M., J. A. Burt, J. A. Burns, M. R. Showalter, (2014b), Non-circular features in Saturn’s D-ring: D68, Icarus, 233, 147−162.

Hedman, M. M. and P. D. Nicholson, (2014), More Kronoseismology with Saturn's rings, Monthly Notices of the Royal Astronomical Society, 444, 1369−1388.

Hedman, M. M., P. D. Nicholson, J. N. Cuzzi, R. N. Clark, G. Filacchione, F. Capaccioni, M. Ciarniello, (2013a), Connections between spectra and structure in Saturn’s main rings based on Cassini VIMS data, Icarus, 223, 105−130.

Hedman, M. M., J. A. Burns, D. P. Hamilton, M. R. Showalter, (2013b), Of horseshoes and heliotropes: Dynamics of dust in the Encke Gap, Icarus, 223, 252−276.

Hedman, M. M. and P. D. Nicholson, (2013), Kronoseismology: Using density waves in Saturn's C-ring to probe the planet's interior, The Astronomical Journal, vol. 146, no. 1, doi: 10.1088/0004-6256/146/1/12.

Hedman, M. M., J. A. Burns, D. P. Hamilton, M. R. Showalter, (2012), The three-dimensional structure of Saturn's E-ring, Icarus, 217, 322−338.

Hedman, M. M., J. A. Burns, P. C. Thomas, M. S. Tiscareno, M. W. Evans, (2011a), Physical properties of the small moon Aegaeon (Saturn LIII), European Planetary Science Congress-

Division for Planetary Sciences (EPSC-DPS) Joint Meeting, 02–07 October 2011, Nantes, France.

Hedman, M. M., P. D. Nicholson, M. R. Showalter, R. H. Brown, B. J. Buratti, R. N. Clark, K. Baines, C. Sotin, (2011b), The Christiansen Effect in Saturn's narrow dusty rings and the spectral identification of clumps in the F-ring, Icarus, 215, 695−711.

Hedman, M. M., J. A. Burns, M. W. Evans, M. S. Tiscareno, C. C. Porco, (2011c), Saturn's curiously corrugated C-ring , Science, 332, 708.

Hedman, M. M., J. A. Burt, J. A. Burns, M. S. Tiscareno, (2010a), The shape and dynamics of a heliotropic dusty ringlet in the Cassini Division, Icarus, 210, 284−297.

Hedman, M. M., P. D. Nicholson, K. H. Baines, B. J. Buratti, C. Sotin, R. N. Clark, R. H. Brown, R. G. French, E. A. Marouf, (2010b), The architecture of the Cassini Division, The Astronomical Journal, 139, 228−251.

Hedman, M. M., N. J. Cooper, C. D. Murray, K. Beurle, M. W. Evans, M. S. Tiscareno, J. A. Burns, (2010c), Aegaeon (Saturn LIII), a G-ring object, Icarus, 207, 433−447.

Hedman, M. M., J. A. Burns, M. S. Tiscareno, C. C. Porco, (2009a), Organizing some very tenuous things: Resonant structures in Saturn's faint rings, Icarus, 202, 260−279.

Hedman, M. M., C. D. Murray, N. J. Cooper, M. S. Tiscareno, K. Beurle, M. W. Evans, J. A. Burns, (2009b), Three tenuous rings/arcs for three tiny moons, Icarus, 199, 378−386.

Hedman, M. M., P. D. Nicholson, H. Salo, B. D. Wallis, B. J. Buratti, K. H. Baines, R. H. Brown, R. N. Clark, (2007a), Self-gravity wake structures in Saturn's A-ring revealed by Cassini VIMS, The Astronomical Journal, 133, 2624–2629.

Hedman, M. M., J. A. Burns, M. R. Showalter, C. C. Porco, P. D. Nicholson, A. S. Bosh, M. S. Tiscareno, et al., (2007b), Saturn's dynamic D-ring, Icarus, 188, 1, 89–107, doi: 10.1016/j.icarus.2006.11.017.

Hedman, M. M., J. A. Burns, M. S. Tiscareno, C. C. Porco, G. H. Jones, E. Roussos, N. Krupp, C. Paranicas, S. Kempf, (2007), The source of Saturn's G ring, Science, 317, no. 5838, 653–656.

Horanyi, M., J. A. Burns, M. M. Hedman, G. H. Jones, S. Kempf, (2009), Diffuse Rings, Chapter 16, In Saturn from Cassini-Huygens, (eds.) M. K. Dougherty, L. W. Esposito, S. M. Krimigis, Springer, Dordrecht, pp. 511–536, doi: 10.1007/978-1-4020-9217-6_16.

Hsu, H.-W., J. Schmidt, S. Kempf, F. Postberg, G. Moragas-Klostermeyer, M. Seiß, H. Hoffmann, et al., (2018), In situ collection of dust grains falling from Saturn's rings into its atmosphere, Science, 362, 6410, doi: 10.1126/science.aat3185.

Iess, L., B. Militzer, Y. Kaspi, P. Nicholson, D. Durante, P. Racioppa, A. Anabtawi, E. Galanti, W. Hubbard, M. J. Mariani, P. Tortora, S. Wahl, M. Zannoni, (2019), Measurement and implications of Saturn's gravity field and ring mass, Science, 364, Issue 6445, eaat2965, doi: 10.1126/science.aat2965.

Jacobson, R. A., J. Spitale, C. C. Porco, K. Beurle, N. J. Cooper, M. W. Evans, C. D. Murray, (2008), Revised orbits of Saturn's small inner satellites, The Astronomical Journal, 135, 261−263.

Jerousek, R. G., J. E. Colwell, L. W. Esposito, P. D. Nicholson, M. M. Hedman, (2016), Small particles and self-gravity wakes in Saturn's rings from UVIS and VIMS stellar occultations, Icarus, 279, 36−50.

Johnson, R. E., W.-L. Tseng, M. K. Elrod, A. M. Persoon, (2017), Nanograin density outside Saturn’s A-ring, The Astrophysical Journal, vol. 834, no. 1, doi: 10.3847/2041-8213/834/1/L6.

Kempf, S., N. Altobelli, J. N. Cuzzi, P. R. Estrada, R. Srama, (2019), Exogenous dust delivery into the Saturnian system constrains ring age to 10**8 years, in preparation.

Kollmann, P., E. Roussos, A. Kotova, L. Regoli, D. G. Mitchell, J. Carbary, G. Clark, N. Krupp, C. Paranicas, (2019), Saturn's innermost radiation belt throughout and inward of the D-ring, Geophysical Research Letters, 45, 10912−10920, doi: 10.1029/2018GL077954.

Lainey, V., R. A. Jacobson, R. Tajeddine, N. J. Cooper, C. Murray, V. Robert, G. Tobie, T. Guillot, S. Mathis, F. Remus, J. Desmars, J.-E. Arlot, J.-P. De Cuyper, V. Dehant, D. Pascu, W. Thuillot, C. Le Poncin-Lafitte, J.-P. Zahn, (2017), New constraints on Saturn's interior from Cassini astrometric data, Icarus, 281, 286−296.

Laughlin, G., V. Korchagin, F. C. Adams, (1997), Spiral mode saturation in self-gravitating disks, The Astrophysical Journal, 477, 410-423.

Leyrat, C., L. J. Spilker, N. Altobelli, S. Pilorz, C. Ferrari, (2008), Infrared observations of Saturn’s rings by Cassini CIRS: Phase angle and local time dependence, Planetary and Space Science, 56, 117–133.

Mankovich, C., M. S. Marley, J. J. Fortney, N. Movshovitz, (2019), Cassini ring seismology as a probe of Saturn’s interior I: Rigid rotation, The Astrophysical Journal, vol. 871, no. 1, doi: 10.3847/1538-4357/aaf798.

Marley, M. S., (2014), Saturn ring seismology: Looking beyond first order resonances, Icarus, 234, 194−199.

Marley, M. S. and C. C. Porco, (1993), Planetary acoustic mode seismology - Saturn's rings, Icarus, 106, 508.

Marley, M, S., (1990), Nonradial oscillations of Saturn: Implications for ring system structure, Ph.D. Thesis, University of Arizona, Tucson.

Marley, M. S., W. B. Hubbard, C. C. Porco, (1989), C-ring features and f-mode oscillations of Saturn, Bulletin of the American Astronomical Society (BAAS) 21, pp. 928.

Marley, M. S., W. B. Hubbard, C. C. Porco, (1987), Saturnian nonradial p-mode oscillations and C-ring structure, Bulletin of the American Astronomical Society (BAAS) 19, pp 889.

Marouf, E. A., R. G. French, N. J. Rappaport, K. Wong, C. McGhee, A. Anabtawi, (2011), Six centuries old spiral of vertical corrugations in Saturn's C-ring, American Geophysical Union (AGU), Fall Meeting, December 3−7, 2011, San Francisco, CA, abstract P12B-01.

McGhee, C. A., R. G. French, L. Dones, J. N. Cuzzi, H. J. Salo, R. Danos, (2005), HST observations of spokes in Saturn's B-ring, Icarus, 173, 508−521.

McGhee, C. A., P. D. Nicholson, R. G. French, K. J. Hall, (2001), HST observations of Saturnian satellites during the 1995 ring plane crossings, Icarus, 152, 282−315.

Meinke, B. K., L. W. Esposito, N. Albers, M. Sremčević, (2012), Classification of F-ring features observed in Cassini UVIS occultations, Icarus, 218, 545−554.

Miller, K. et al., (2019), in preparation.

Mitchell, C. J., C. C. Porco, J. W. Weiss, (2015), Tracking the Geysers of Enceladus into Saturn's E-ring, The Astronomical Journal, vol. 149, no. 5, doi: 10.1088/0004-6256/149/5/156.

Mitchell, C. J., C. C. Porco, H. L. Dones, J. N. Spitale, (2013), The behavior of spokes in Saturn's B-ring, Icarus, 225, 446−474.

Mitchell, C. J., M. Horányi, O. Havnes, C. C. Porco, (2006), Saturn's spokes: Lost and found, Science, 311, 1587−1589.

Mitchell, D. G., M. E. Perry, D. C. Hamilton, J. H. Westlake, P. Kollmann, H. T. Smith, J. F. Carbary, et al., (2018), Dust grains fall from Saturn's D-ring into its equatorial upper atmosphere, Science, 362, 6410, doi: 10.1126/science.aat2236.

Morishima, R., N. Turner, L. Spilker, (2017), Surface roughness of Saturn's rings and ring particles inferred from thermal phase curves, Icarus, 295, 74–88.

Morishima, R., L. Spilker, S. Brooks, E. Deau, S. Pilorz, (2016), Incomplete cooling down of Saturn's A-ring at solar equinox: Implication for seasonal thermal inertia and internal structure of ring particles, Icarus, 279, 2–19.

Morishima, R., L. Spilker, N. Truner, (2014), Azimuthal temperature modulations of Saturn's A-ring caused by self-gravity wakes, Icarus, 228, 247–259.

Morishima, R., S. G., Edgington, L. Spilker, (2012), Regolith grain sizes of Saturn's rings inferred from Cassini-CIRS far-infrared spectra, Icarus, 221, 888–899.

Morishima, R., L. Spilker, H. Salo, et al., (2010), A multilayer model for thermal infrared emission of Saturns rings II: Albedo, spins, and vertical mixing of ring particles inferred from Cassini CIRS, Icarus, 210, 330–345.

Murray, C. D. and R. C. French, (2018), The F-ring, Chapter 13, In Planetary Rings, (eds.) M. Tiscareno, C. Murray, Cambridge University Press, pp. 338−362, doi: 10.1017/9781316286791.013.

Murray, C. D., N. J. Cooper, G. A. Williams, N. O. Attree, J. S. Boyer, (2014), The discovery and dynamical evolution of an object at the outer edge of Saturn's A-ring, Icarus, 236, 165−168.

Murray, C. D., K. Beurle, N. J. Cooper, M. W. Evans, G. A. Williams, S. Charnoz, (2008), The determination of the structure of Saturn's F-ring by nearby moonlets, Nature, 453, 7196, 739−744.

Murray, C. D., C. Chavez, K. Beurle, N. Cooper, M. W. Evans, J. A. Burns, C. C. Porco, (2005), How Prometheus creates structure in Saturn's F-ring, Nature, 437, 1326−1329.

Nicholson, P. D., R. G. French, J. N. Spitale, (2018), Narrow rings, gaps and sharp edges, Chapter 11, In Planetary Rings, (eds.) M. Tiscareno and C. Murray, Cambridge University Press, pp. 276−307, doi: 10.1017/9781316286791.011.

Nicholson, P. D., R. G. French, M. M. Hedman, et al., (2014), Noncircular features in Saturn's rings I: The edge of the B-ring, Icarus, 227, 152−175.

Nicholson, P. D. and M. M. Hedman, (2010), Self-gravity wake parameters in Saturn's A- and B-rings, Icarus, 206, 410−423.

Nicholson, P. D., M. M. Hedman, R. N. Clark, M. R. Showalter, D. P. Cruikshank, J. N. Cuzzi, G. Filacchione, F. Capaccioni, P. Cerroni, G. B. Hansen, B. Sicardy, P. Drossart, R. H. Brown, B. J. Buratti, K. H. Baines, A. Coradini, (2008), A close look at Saturn's rings with Cassini VIMS, Icarus, 193, 182−212.

Nitter, T., O. Havnes, F. Melandsø, (1998), Levitation and dynamics of charged dust in the photoelectron sheath above surfaces in space, Journal of Geophysical Research, 103, 6605−6620.

Nixon, C. A., R. D. Lorenz, R. K. Achterberg, A. Buch, P. Coll, R. N. Clark, R. Courtin, A. Hayes, L. Iess, R. E. Johnson, R. M. C. Lopes, M. Mastrogiuseppe, K. Mandt, D. G. Mitchell, F. Raulin, A. M. Rymer, H. T. Smith, A. Solomonidou, C. Sotin, D. Strobel, et al., (2018), Titan's cold case files - Outstanding questions after Cassini-Huygens, Planetary and Space Science, 155, 50−72, doi: 10.1016/j.pss.2018.02.009.

O'Donoghue, J., L. Moore, J. Connerney, H. Melin, T. S. Stallard, S. Miller, K. H. Baines, (2019), Observations of the chemical and thermal response of 'ring rain' on Saturn's ionosphere Icarus, 322, 251−260, doi: 10.1016/j.icarus.2018.10.027.

Orton, G. S., K. H. Baines, D. Cruikshank, J. N. Cuzzi, S. M. Krimigis, S. Miller, E. Lellouch, (2009), Review of knowledge prior to the Cassini-Huygens Mission and concurrent research, Chapter 2, In Saturn from Cassini-Huygens, (eds.) M. K. Dougherty, L. W. Esposito, S. M. Krimigis, Springer, Dordrecht, pp. 9−54, doi: 10.1007/978-1-4020-9217-6_2.

Pan, M., H. Rein, E. Chiang, S. N. Evans, (2012), Stochastic flights of propellers, Monthly Notices of the Royal Astronomical Society, vol. 427, Issue 4, pp. 2788−2796, doi: 10.1111/j.1365-2966.2012.22023.x.

Pan, M. and E. Chiang, (2012), Care and feeding of frogs, The Astronomical Journal, vol. 143, no. 1, doi: 10.1088/0004-6256/143/1/9.

Pan, M. and E. Chiang, (2010), The propeller and the frog, The Astrophysical Journal, vol. 722, no. 2, doi: 10.1088/2041-8205/722/2/L178.

Perry, M. E., J. H. Waite Jr., D. G. Mitchell, K. E. Miller, T. E. Cravens, R. S. Perryman, L. Moore, et al., (2018), Material flux from the rings of Saturn into its atmosphere, Geophysical Research Letters, vol. 45, Issue 19, pp. 10,093−10,100, doi: 10.1029/2018GL078575.

Pilorz, S., N. Altobelli, J. Colwell, M. Showalter, (2015), Thermal transport in Saturn’s B-ring inferred from Cassini CIRS, Icarus, 254, 157–177.

Porco, C. C., J. W. Weiss, D. C. Richardson, L. Dones, T. Quinn, H. Throop, (2008), Simulations of the dynamical and light-scattering behavior of Saturn's rings and the derivation of ring particle and disk properties, The Astronomical Journal, vol. 136, no. 5, pp. 2172–2200, doi: 10.1088/0004-6256/136/5/2172.

Porco, C. C., P. C. Thomas, J. W. Weiss, D. C. Richardson, (2007) Saturn’s small inner satellites: Clues to their origins, Science, 318, 1602.

Porco, C. C., E. Baker, J. Barbara, K. Beurle, A. Brahic, J. A. Burns, S. Charnoz, N. Cooper, D. D. Dawson, A. D. Del Genio, T. Denk, L. Dones, U. Dyudina, M. W. Evans, B. Giese, K. Grazier, P. Helfenstein, A. P. Ingersoll, R. A. Jacobson, T. V. Johnson, A. McEwen, C. D. Murray, G. Neukum, W. M. Owen, J. Perry, T. Roatsch, J. Spitale, S. Squyres, P. Thomas, M. Tiscareno, E. Turtle, A. R. Vasavada, J. Veverka, R. Wagner, R. West, (2005), Cassini imaging science: Initial results on Saturn's rings and small satellites, Science, 307, 5713, 1226−1236.

Porco, C. C., R. A. West, A. McEwen, A. D. Del Genio, A. P. Ingersoll, P. Thomas, S. Squyres, L. Dones, C. D. Murray, T. V. Johnson, J.A. Burns, A. Brahic, G. Neukum, J. Veverka, J. M. Barbara, T. Denk, M. Evans, J. J. Ferrier, P. Geissler, P. Helfenstein, T. Roatsch, H. Throop, M. Tiscareno, A. R. Vasavada, (2003), Cassini imaging of Jupiter's atmosphere, satellites, and rings, Science, 299, no. 5612, 1541−1547.

Porco, C., G. E. Danielson, P. Goldreich, J. B. Holberg, A. L. Lane, (1984), Saturn's nonaxisymmetric ring edges at 1.95 R_s and 2.27 R_s, Icarus, 60, 17−28.

Poulet, F., D. P. Cruikshank, J. N. Cuzzi, T. L. Roush, R. G. French, (2003), Compositions of Saturn's rings A, B, and C from high resolution near-infrared spectroscopic observations, Astronomy & Astrophysics, 412, 305−316.

Poulet, F. and J. N. Cuzzi, (2002), The Composition of Saturn's Rings, Icarus, 160, 350−358.

Poulet, F. and B. Sicardy, (2001), Dynamical evolution of the Prometheus-Pandora system, Monthly Notices of the Royal Astronomical Society, vol. 322, pp 343−355.

Reffet, E., M. Verdier, C. Ferrari, (2015) Thickness of Saturn’s B-ring as derived from seasonal temperature variations measured by Cassini CIRS, Icarus, 254, 276–286.

Rein, H. and J. C. B. Papaloizou, (2010), Stochastic orbital migration of small bodies in Saturn's rings, Astronomy & Astrophysics, 524, A22, doi: 10.1051/0004-6361/201015177.

Robbins, S. J., G. R. Stewart, M. C. Lewis, J. E. Colwell, M. Sremcević, (2010), Estimating the masses of Saturn’s A- and B-rings from high-optical depth N-body simulations and stellar occultations, Icarus, 206, 431–445.

Rosen, P. A., G. L. Tyler, E. A. Marouf, J. J. Lissauer, (1991), Resonance structures in Saturn's rings probed by radio occultation II: Results and interpretation, Icarus, 93, 1, 25−44.

Roussos, E., P. Kollmann, N. Krupp, A. Kotova, L. Regoli, C. Paranicas, D. G. Mitchell, S. M. Krimigis, D. Hamilton, P. Brandt, J. Carbary, S. Christon, K. Dialynas, I. Dandouras, M. E. Hill, W. H. Ip, G. H. Jones, S. Livi, B. H. Mauk, B. Palmaerts, et al., (2019), A radiation belt of energetic protons located between Saturn and its rings, Science, vol. 362, Issue 6410, eaat1962, doi: 10.1126/science.aat1962.

Salo, H. and R. G. French, (2010), The opposition and tilt effects of Saturn’s rings from HST observations, Icarus, 210, 785−816.

Schaffer, L. and J. A. Burns, (1987), The dynamics of weakly charged dust - Motion through Jupiter's gravitational and magnetic fields, Journal of Geophysical Research, 92, 2264−2280.

Schmidt, J., J. E. Colwell, M. Lehmann, E. A. Marouf, H. Salo, F. Spahn, M. S. Tiscareno, (2016), On the linear damping relation for density waves in Saturn's rings, The Astrophysical Journal, vol. 824, no. 1, doi: 10.3847/0004-637X/824/1/33.

Schmidt, J. and M. S. Tiscareno, (2013), Ejecta clouds from meteoroid impacts on Saturn's rings: Constraints on the orbital elements and size of the projectiles, American Geophysical Union (AGU), Fall Meeting, abstract P23D-1820.

Schmidt, J., K. Ohtsuki, N. Rappaport, H. Salo, F. Spahn, (2009), Dynamics of Saturn's dense rings, In Saturn from Cassini-Huygens, Chapter 14, (eds.) M. K. Dougherty, L. W. Esposito, S. M. Krimigis, Springer, Dordrecht, pp. 413−458, doi: 10.1007/978-1-4020-9217-6_14.

Seiler, M., M. Sremčević, M. Seiß, H. Hoffmann, F. Spahn, (2017), A librational model for the propeller Blériot in the Saturnian ring system, The Astrophysical Journal, vol. 840, no. 2, doi: 10.3847/2041-8213/aa6d73.

Seiß, M., N. Albers, M. Sremčević, J. Schmidt, H. Salo, M. Seiler, H. Hoffmann, F. Spahn, (2018), Hydrodynamic simulations of moonlet-induced propellers in Saturn's rings: Application to Blériot, The Astronomical Journal, vol 157, no. 1, doi: 10.3847/1538-3881/aaed44.

Shimizu, M., (1982), Strong interaction between the ring system and the ionosphere of Saturn, Moon and the Planets, 22, pp. 521−522.

Showalter, M. R., (1991), Visual detection of 1981S13, Saturn's eighteenth satellite, and its role in the Encke gap, Nature, 351, 709−713.

Showalter, M. R. and P. D. Nicholson, (1990), Saturn's rings through a microscope - Particle size constraints from the Voyager PPS scan, Icarus, 87, 285−306.

Shu, F. H., (1984), Waves in planetary rings, Chapter 9, In Planetary Rings, (A85-34401 15-88), (eds.) R. Greenberg, A. Brahic, University of Arizona Press, pp. 513−561.

Smith, B. A., L. Soderblom, R. M. Batson, P. M. Bridges, J. L. Inge, H. Masursky, E. Shoemaker, R. F. Beebe, J. Boyce, G. Briggs, A. Bunker, S. A. Collins, C. Hansen, T. V. Johnson, J. L. Mitchell, R. J. Terrile, A. F. Cook, J. N. Cuzzi, J. B. Pollack, G. E. Danielson, A. P. Ingersoll, M. E. Davies, G. E. Hunt, D. Morrison, T. Owen, C. Sagan, J. Veverka, R. Strom, V. E. Suomi, (1982), A new look at the Saturn system - The Voyager 2 images, Science, 215, 504−537.

Spahn, F., H. Hoffmann, H. Rein, M. Seiß, M. Sremčević, M. Tiscareno, (2018), Moonlets in dense planetary rings, Chapter 8, In Planetary Ring Systems, (eds.) M. Tiscareno, C. Murray, Cambridge University Press, pp. 157−197, doi: 10.1017/9781316286791.008.

Spahn, F., H. Scholl, J.-M. Hertzsch, (1994), Structures in planetary rings caused by embedded moonlets, Icarus, 111, 514−535.

Spilker, L. J., C. Ferrari, N. Altobelli, S. Pilorz, R. Morishima, (2018), Thermal properties of rings and ring particles, Chapter 15, In Planetary Ring Systems, (eds.) M. Tiscareno, C. Murray, Cambridge University Press, pp. 399−433, doi: 10.1017/9781316286791.015.

Spilker, L. J., S. H. Pilorz, S. G. Edgington, et al., (2005), Cassini CIRS observations of a roll-off in Saturn ring spectra at submillimeter wavelengths, Earth Moon Planets, 96, 149–163.

Spitale, J. N., (2017), Saturn's misbegotten moonlets, American Astronomical Society (AAS), Division on Dynamical Astronomy (DDA), meeting 48, id. 400.04.

Spitale, J. N. and J. M. Hahn, (2016), The shape of Saturn's Huygens ringlet viewed by Cassini ISS, Icarus, 279, 141−154.

Spitale, J. N. and C. C. Porco, (2010), Detection of free unstable modes and massive bodies in Saturn's outer B-ring, The Astronomical Journal, vol. 140, no. 6, pp. 1747−1757, doi: 10.1088/0004-6256/140/6/1747.

Spitale, J. N. and C. C. Porco, (2009), Time variability in the outer edge of Saturn's A-ring revealed by Cassini imaging, The Astronomical Journal, vol. 138, no. 5, pp. 1520−1528, doi: 10.1088/0004-6256/138/5/1520.

Spitale, J. N., R. A. Jacobson, C. C. Porco, W. M. Owen Jr., (2006), The orbits of Saturn's small satellites derived from combined historic and cassini imaging observations, The Astronomical Journal, vol. 132, no. 2, pp. 692−710.

Srama, R., M. Burton, S. Helfert, S. Kempf, G. Moragas-Klostermeyer, A. Mocker, F. Postberg, M. Roy, E. Grün, (2005), Cassini Saturn dust measurements, Workshop on Dust in Planetary Systems, Kaua‘i, HI, Sep. 26–30, 2005, LPI Contribution No. 1280, p. 133, https://www.lpi.usra.edu/lpi/contribution_docs/LPI-001280.pdf.

Sremčević, M., G. R. Stewart, N. Albers, L. W. Esposito, (2014a), Propellers in Saturn's rings, European Planetary Science Congress (EPSC), Abstract, vol. 9, id. EPSC2014-633.

Sremčević, M., G. R. Stewart, N. Albers, L. W. Esposito, (2014b), Propellers in Saturn A- and B-rings, American Astronomical Society (AAS), Division for Planetary Sciences (/DPS) 46th Annual Meeting, November 9−14, 2014, Tucson, AZ, meeting 46, id. 417.01.

Sremčević, M., G. R. Stewart, N. Albers, L. W. Esposito, (2013), Propellers in Saturn's rings American Geophysical Union (AGU), Fall Meeting, December 9−13, 2013, San Francisco, CA, abstract P21E-07.

Sremčević, M., G. R. Stewart, N. Albers, L. W. Esposito, (2012), Discovery of B-ring propellers In Cassini UVIS and ISS, American Astronomical Society (AAS), Division for Planetary Sciences (DPS), October 14−19, 2012, Reno, NV, meeting 44, id. 513.06.

Sremčević, M., J. Schmidt, H. Salo, M. Seisz, F. Spahn, N. Albers, (2007), A belt of moonlets in Saturn's A-ring, Nature, 449, 1019−1021.

Sremčević, M., A. V. Krivov, H. Krüger, F. Spahn, (2005), Impact-generated dust clouds around planetary satellites: Model versus Galileo data, Planetary and Space Science, 53, 625−641.

Tajeddine, R., P. D. Nicholson, P.-Y. Longaretti, M. El Moutamid, J. A. Burns, (2017a), What Confines the Rings of Saturn?, The Astrophysical Journal Supplement Seried, vol. 232, no. 2, doi: 10.3847/1538-4365/aa8c09.

Tajeddine, R., P. D. Nicholson, M. S. Tiscareno, M. M. Hedman, J. A. Burns, M. El Moutamid, (2017b), Dynamical phenomena at the inner edge of the Keeler gap, Icarus, 289, 80−93.

Tajeddine, R., V. Lainey, N. J. Cooper, C. D. Murray, (2013), Cassini ISS astrometry of the Saturnian satellites: Tethys, Dione, Rhea, Iapetus, and Phoebe 2004−2012, Astronomy & Astrophysics, 575, A73, doi: 10.1051/0004-6361/201425605.

- - - - - - - - - - - - - -

Tamayo, D., S. R. Markham, M. M. Hedman, J. A. Burns, D. P. Hamilton, (2016), Radial profiles of the Phoebe ring: A vast debris disk around Saturn, Icarus, 275, 117−131.

Tamayo, D., M. M. Hedman, J. A. Burns, (2014), First observations of the Phoebe ring in optical light, Icarus, 233, pp. 1−8.

Thomson, F. S., E. A. Marouf, G. L. Tyler, R. G. French, N. J. Rappoport, (2007), Periodic microstructure in Saturn's rings A and B, Geophysical Research Letters, vol. 34, Issue 24, doi: 10.1029/2007GL032526|.

Throop, H. B., C. C. Porco, R. A. West, J. A. Burns, M. R. Showalter, P. D. Nicholson, (2004), The Jovian rings: New results derived from Cassini, Galileo, Voyager, and Earth-based observations, Icarus, 172, 59−77.

Tiscareno, M. S., P. D. Nicholson, J. N. Cuzzi, L. J. Spilker, C. D. Murray, M. M. Hedman, J. E. Colwell, J. A. Burns, S. M. Brooks, R. N. Clark, N. J. Cooper, E. Deau, C. Ferrari, G. Filacchione, R. G. Jerousek, S. Le Mouélic, R. Morishima, S. Pilorz, S. Rodriguez, M. R. Showalter, (2019a), Close-range remote sensing of Saturn's rings during Cassini's ring-grazing orbits and Grand Finale, Science, vol. 364, Issue 6445, eaau1017, doi: 10.1126/science.aau1017.

Tiscareno, M. S., P. D. Nicholson, J. N. Cuzzi, L. J. Spilker, C. D. Murray, M. M. Hedman, J. E. Colwell, et al., (2019b), Close-range remote sensing of Saturn’s rings during Cassini’s ring-grazing orbits and Grand Finale, Science, vol. 364, no. 6445, eaau1017, doi: 10.1126/science.aau1017.

Tiscareno, M. S. and B. E. Harris, (2018), Mapping spiral waves and other radial features in Saturn's rings, Icarus, 312, 157−171, doi: 10.1016/j.icarus.2018.04.023.

Tiscareno, M. S., M. M. Hedman, J. A. Burns, J. W. Weiss, C. C. Porco, (2013a), Probing the inner boundaries of Saturn's A-ring with the Iapetus -1:0 nodal bending wave, Icarus, 224, 201−208.

Tiscareno, M. S., C. J. Mitchell, C. D. Murray, D. Di Nino, M. M. Hedman, J. Schmidt, J. A. Burns, J. N. Cuzzi, C. C. Porco, K. Beurle, M. W. Evans, (2013b), Observations of ejecta clouds produced by impacts onto Saturn’s rings, Science, 340, Issue 6131, 460−464.

Tiscareno, M. S., (2013), A modified “Type I migration” model for propeller moons in Saturn's rings, Planetary and Space Science, 77, 36−142.

Tiscareno, M. S., J. A. Burns, M. Sremčević, K. Beurle, M. M. Hedman, N. J. Cooper, A. J. Milano, M. W. Evans, C. C. Porco, J. N. Spitale, J. W. Weiss, (2010), Physical characteristics and non-keplerian orbital motion of "propeller" moons embedded in Saturn's rings, The Astrophysical Journal, vol. 718, no. 2, doi: 10.1088/2041-8205/718/2/L92.

Tiscareno, M. S., J. A. Burns, M. M. Hedman, C. C. Porco, (2008), The population of propellers in Saturn's A-ring, The Astronomical Journal, vol. 135, no. 3, pp. 1083−1091, doi: 10.1088/0004-6256/135/3/1083.

Tiscareno, M. S., J. A. Burns, P. D. Nicholson, M. M. Hedman, C. C. Porco, (2007), Cassini imaging of Saturn's rings II: A wavelet technique for analysis of density waves and other radial structure in the rings, Icarus, 189, 14−34.

Tiscareno, M. S., J. A. Burns, M. M. Hedman, C. C. Porco, J. W. Weiss, L. Dones, D. C. Richardson, C. D. Murray, (2006), 100-metre-diameter moonlets in Saturn's A-ring from observations of ‘propeller’ structures, Nature, 440, Issue 7084, 648−650.

Tseng, W.-L., R. E. Johnson, M. K. Elrod, (2013), Modeling the seasonal variability of the plasma environment in Saturn's magnetosphere between main rings and Mimas, Planetary and Space Science, 77, 126−135.

Tseng, W.-L., W.-H. Ip, R. E. Johnson, T. A. Cassidy, M. K. Elrod, (2010), The structure and time variability of the ring atmosphere and ionosphere, Icarus, 206, 382−389.

Vahidinia, S., J. N. Cuzzi, M. Hedman, B. Draine, R. N. Clark, T. Roush, G. Filacchione, P. D. Nicholson, R. H. Brown, B. Buratti, C. Sotin, (2011), Saturn's F-ring grains: Aggregates made of crystalline water ice, Icarus, 215, Issue 2, pp. 682−694.

Van Allen, J. A., (1982), Findings on rings and inner satellites of Saturn of Pioneer 11, Icarus, 51, 509−527.

Verbiscer, A. J., M. F. Skrutskie, D. P. Hamilton, (2009), Saturn's largest ring, Nature, 461, 1098−1100.

Waite Jr., J. H., R. Perryman, M. Perry, K. Miller, J. Bell, T. E. Cravens, C. R. Glein, J. Grimes, M. Hedman, J. Cuzzi, T. Brockwell, B. Teolis, L. Moore, D. Mitchell, A. Persoon, W. S. Kurth, J.-E. Wahlund, M. Morooka, L. Hadid, S. Chocron, J. Walker, A. Nagy, R. Yelle, S. Ledvina, R. Johnson, W. Tseng, O. J. Tucker, W.-H. Ip, (2018), Chemical interactions between Saturn’s atmosphere and its rings, Science, vol. 362, Issue 6410, eaat2382, doi: 10.1126/science.aat2382.

Weiss, J. W., C. C. Porco, M. S. Tiscareno, (2009), Ring edge waves and the masses of nearby satellites, The Astronomical Journal, vol. 138, no. 1, pp. 272−286, doi: 10.1088/0004-6256/138/1/272.

Ye, S. Y., D. A. Gurnett, W. S. Kurth, (2016), In-situ measurements of Saturn's dusty rings based on dust impact signals detected by Cassini RPWS, Icarus, 279, 51−61.

Zebker, H. A., E. A. Marouf, G. L. Tyler, (1985), Saturn's rings - Particle size distributions for thin layer model, Icarus, 64, 531−548.

Zhang, Z., A. G. Hayes, I. de Pater, D. E. Dunn, M. A. Janssen, P. D. Nicholson, J. N. Cuzzi, B. J. Butler, R. J. Sault, S. Chatterjee, (2019), VLA multi-wavelength microwave observations of Saturn's C- and B-rings, Icarus, 317, 518−548, doi: 10.1016/j.icarus.2018.08.014.

Zhang, Z., A. G. Hayes, M. A. Janssen, P. D. Nicholson, J. N. Cuzzi, I. de Pater, D. E. Dunn, P. R. Estrada, M. M. Hedman, (2017a), Cassini microwave observations provide clues to the origin of Saturn's C-ring, Icarus, 281, 297−321.

Zhang, Z., A. G. Hayes, M. A. Janssen, P. D. Nicholson, J. N. Cuzzi, I. de Pater, D. E. Dunn, (2017b), Exposure age of Saturn's A- and B-rings, and the Cassini Division as suggested by their non-icy material content, Icarus, 294, 14−42.